Dynamics of magmatic intrusions in the upper crust: Theory and applications to laccoliths on Earth and the Moon

Chloé Michaut

Dynamics of magmatic intrusions in the upper crust: Theory and applications to laccoliths on Earth and the Moon

Chloé Michaut[1]

Received 18 November 2010; revised 11 February 2011; accepted 23 February 2011; published 17 May 2011.

[1] To understand the dynamics of shallow magmatic intrusions, I propose a theoretical model of magma spreading laterally below an elastic crust. Nondimensionalization of the flow equation leads to the identification of characteristic scales for the intrusion: while the characteristic intrusion length is controlled by the elastic response of the crust, its characteristic thickness primarily depends on magma properties and injection rate. Three spreading regimes are identified and characterized by different morphologies as well as by scaling laws for thickness versus length and thickness versus time. The first spreading regime is controlled by the elastic response of the crust and the shape of the flow is self-similar. When the time, length, and thickness become larger than an elastic time, length, and thickness scale, the edges of the flow become steeper and the system transitions to a gravity current regime. When the intrusion is thick enough to accommodate the pressure head, the flow enters a regime of lateral propagation and keeps a constant thickness. The intrusion shape in the elastic regime fits the observed shape of terrestrial laccoliths. The elastic scaling law for intrusion thickness versus length fits observations of laccoliths at Elba Island, Italy, and provides for a physical explanation for the observed relationship between length and thickness on terrestrial laccoliths. Laccoliths are predicted to form over short time scales, depending on magma viscosity, that vary between approximately a month to several years for felsic magmas on Earth. On the Moon, several elongated low-slope domes have recently been identified as possibly formed by laccolith intrusions at depth, although they are much larger than terrestrial laccoliths. Because the Moon has a smaller gravity than on the Earth, a deeper magma source, and a more mafic magma composition than for terrestrial laccoliths (implying smaller pressure gradient and dike width), lunar intrusions have a larger characteristic length and a smaller characteristic thickness. After nondimensionalization, the morphologies (length versus thickness) of terrestrial and inferred lunar laccoliths follow the same curve and are well fitted by the elastic scaling law. This model thus explains the size discrepancy between terrestrial laccoliths and lunar low-slope domes. Therefore, low-slope domes identified on the Moon are good candidates for laccolith-type intrusions at depth.

Citation: Michaut, C. (2011), Dynamics of magmatic intrusions in the upper crust: Theory and applications to laccoliths on Earth and the Moon, *J. Geophys. Res.*, *116*, B05205, doi:10.1029/2010JB008108.

1. Introduction

[2] Magma intrusions in the crust are the first steps of magma reservoir formation. Large magma reservoirs and plutons indeed probably grow by small increments over long time scales [*Petford et al.*, 1993, 1994; *Petford and Gallagher*, 2001; *Annen and Sparks*, 2002; *Glazner et al.*, 2004; *Michaut and Jaupart*, 2006, 2011]. Long-term rates of magma transfer to the crust are quite well constrained [*Crisp*, 1984; *Jellinek and de Paolo*, 2003]. But the formation of large magma reservoirs still poses some challenging questions as most of the thermal models explaining the formation of large volumes of melt require large transient magma input rates, much larger than long-term rates estimated from active and fossil systems [*Annen*, 2009; *Bachmann and Bergantz*, 2003; *Michaut and Jaupart*, 2011]. The rate at which a single intrusion is transferred to the crust is thus crucial to determine the validity of these models.

[3] The dynamics of buoyancy-driven dike propagation in an elastic medium has been well studied [*Lister and Kerr*, 1991; *Rubin*, 1995]. In particular, *Lister and Kerr* [1991] have shown that, except at the dike tips where the elastic forces are important, the dynamics of magma in feeder dikes is controlled by a local balance between buoyancy forces and viscous pressure drop. At the level of neutral

[1]Equipe de Géophysique Spatiale et Planétaire, Institut de Physique du Globe de Paris, UMR 7154, CNRS, Université Paris Diderot, Sorbonne Paris Cité, Saint-Maur-des-Fossés, France.

0148-0227/11/2010JB008108

buoyancy, dikes transition to sills or laccoliths. At large depth in the crust, the dynamics of sills and dikes are comparable [*Lister and Kerr*, 1991]. At shallow depth, however, geological and structural studies on laccoliths have shown that roof lifting is the dominant process by which magma makes room for itself and that the elastic deformation of the overlying crust is crucial in controlling the shape of laccoliths [*Pollard and Johnson*, 1973; *Jackson and Pollard*, 1988]. Most of the research on shallow horizontal magmatic intrusions have thus focused on the geometry of sill or laccolith formation, i.e., on the static elastic deformation induced by the presence of a horizontal intrusion [*Johnson and Pollard*, 1973; *Turcotte and Schubert*, 1982]. Little attention has been given to the dynamics and evolution of such intrusions, i.e., to the fact that magma propagates and that flow length evolves with time. Crack propagation in a semi-infinite elastic medium has been modeled by *Fialko* [2001] and *Kavanagh et al.* [2006] have studied sill formation and crack propagation experimentally as a function of the mechanical properties of the host medium. However, magma viscosity and injection rate necessarily influence the dynamics of sills and laccoliths. The own weight of the magma also induces a hydrostatic pressure gradient through thickening which adds to the driving pressure and must influence the spreading of the flow [*Huppert*, 1982].

[4] In the absence of a physical model for shallow horizontal intrusion dynamics, the geometry of intermediate-scale intrusions can provide some insights into their emplacement and growth processes. Using the comprehensive data sets of *Corry* [1988] on laccolith dimensions, *McCaffrey and Petford* [1997] proposed an empirical power law distribution for laccolith thickness T as a function of length L_d of the form $T = 0.12\ L_d^{0.88}$. The power law exponent value, smaller than 1, is interpreted as reflecting the need for a magma sheet to travel laterally some distance before undergoing vertical thickening [*McCaffrey and Petford*, 1997]. This interpretation is in agreement with field studies that describe laccolith growth as a two-stage process, implying, first, lateral spreading of a sill with very large aspect ratio and, second, vertical thickening of the intrusion by roof lifting [*Johnson and Pollard*, 1973; *Corry*, 1988].

[5] Recent data on laccolith dimensions also show the same kind of power law relationships, but with an exponent larger than 1 and up to 1.5 which has been interpreted as reflecting the vertical inflation stage during laccolith growth [*Rocchi et al.*, 2002; *Mazzarini et al.*, 2004; *Westerman et al.*, 2004; *Corazzato and Gropelli*, 2004].

[6] *Cruden and McCaffrey* [2002] gathered data on intrusion dimensions from small-scale elastic cracks to large-scale batholithic intrusions and proposed that the thickness versus length of felsic to intermediate intrusions follows an S-shaped distribution (in a logarithmic scale) with a maximum slope of ~1.5 for intrusion lengths typical of laccoliths. However, there is no physical framework to explain the origin of this distribution.

[7] At the surface of terrestrial planets, shallow magmatic intrusions have been proposed to explain the relatively high topography and fractured floor of some craters on the Moon, Mars and recently on Mercury [*Schultz*, 1976; *Head et al.*, 2009] as well as low-slope domes on the Moon [*Wöhler et al.*, 2009]. The topographic deformation that could be caused by shallow intrusions can be constrained by observations of planetary surfaces; that is, volume, shape and other dimensions of intrusions can be quantified. But such observations must be linked to models of magma intrusion dynamics in order to provide insights into magma physical properties and injection rate.

[8] In this paper, I develop a theoretical model for the spreading of shallow depth intermediate-scale intrusions, where magma, that is continuously injected at the intrusion center, is accommodated by roof lifting. The model differs from the classical static laccolith model of *Turcotte and Schubert* [1982] in that the length of the flow is self consistently determined. The own weight of the magma was neglected in previous models on laccolith growth [*Kerr and Pollard*, 1998]; it is taken into account here as it also induces pressure gradients that drive the flow horizontally.

[9] Depending on the injection rate, the overlying crust thickness and elasticity as well as magma viscosity and density, three different spreading regimes are identified and characterized by specific morphologies and scaling laws for intrusion thickness versus length and time. Available data on terrestrial laccolith morphologies as well as on candidate intrusive domes on the Moon are compared with these scaling laws and interpreted within the physical framework of this model. Implications of this model are discussed in terms of intrusion thickness and time scale of emplacement. The effects of cooling on flow dynamics are also evaluated.

2. Shallow Magmatic Intrusions

[10] At shallow depth in the upper crust, roof lifting is the dominant process by which magma makes room for itself [*Pollard and Johnson*, 1973; *Jackson and Pollard*, 1988], which leads to the deformation and bending of the overlying strata.

[11] Numerous field and geochronological studies indicate that large-scale intrusions such as plutons, batholiths and magma chambers form and grow by increments of small magma pulses over very long time scales of 10^5 to $>10^6$ years [*Petford et al.*, 1993, 1994; *Metz and Mahood*, 1991; *Sisson et al.*, 1996; *Coleman et al.*, 2004]. In this paper, I focus on intermediate-scale intrusions such as sills, laccoliths and bysmaliths. Some geological studies also suggest that intermediate-scale intrusions form by amalgamation of small magma sheets [*Habert and de Saint-Blanquat*, 2004; *Horsman et al.*, 2005]. However, such studies also show that the emplacement of these intrusions must occur over a short enough time scale for the intrusion to keep a melted core. In the Black Mesa intrusion for instance, solid state textures around internal contacts between sheets are absent and contact metamorphism at the periphery of the intrusion is not significant; *Habert and de Saint-Blanquat* [2004] thus estimated that this body formed in less than ~100 years. Hence, if intermediate-scale intrusions form by amalgamation of small sheets, with a short repose time interval between intrusions, (i.e., such that a melted zone still exists), then the whole intrusion behaves and deforms as a single flow. A characteristic injection rate for the intrusion is

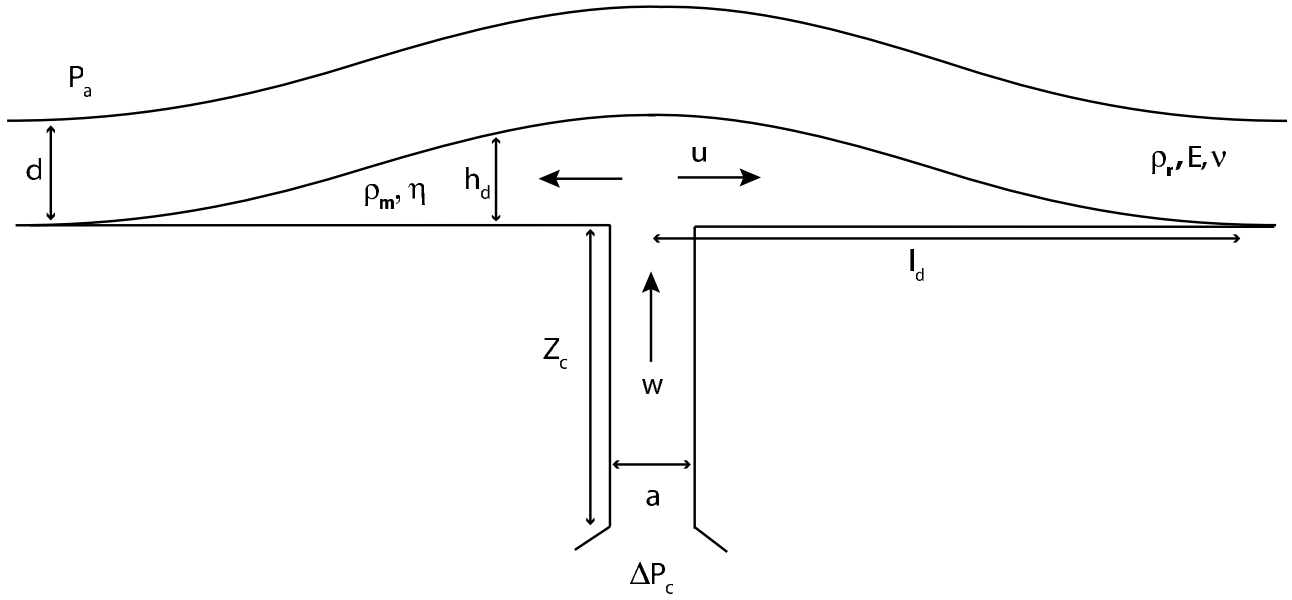

Figure 1. Sketch showing the 2-D geometry and physical properties of the system. Parameters are listed in Table 1.

then simply an average over the whole duration of the emplacement process.

3. A Two-Dimensional Model for Magmatic Intrusions at Shallow Depth

[12] The model developed herein treats the spreading of an isoviscous magma along a weak bedding plane, below a thin elastic crust of constant thickness d and above a rigid layer, situated at $z = 0$. Magma is injected continuously at the base and center of the intrusion and the initial rate of injection Q_0 is determined by the initial overpressure driving the flow in the feeder conduit. As the intrusion weight increases, the overpressure driving magma flow and hence the rate of injection decrease. In order to take this effect into account, the feeder conduit is schematically represented by a dike of width a and length Z_c, infinitely long in the y direction (Figure 1). Intrusion thickness h varies with time and horizontal coordinates. In Appendix B, I consider the case of an axisymmetric intrusion, with injection through a circular conduit.

3.1. Equations of Motion

3.1.1. Momentum Equations

[13] Horizontal motion is similar to the flow in a thin channel, with a characteristic length Λ much larger than the characteristic thickness H of the flow. Consequently, the classical lubrication theory applies, as in the gravity current problem [*Huppert*, 1982]. Horizontal velocities are much larger in magnitude than vertical velocities and horizontal variations in stress and velocity are negligible compared to vertical variations.

[14] Consequently, many simplifications can be made from the full Navier-Stokes equations (see *Huppert* [1982] and *Michaut and Bercovici* [2009] for more details), and conservation of momentum in the horizontal (x) and vertical (z) direction reduces to

$$-\frac{\partial P}{\partial x} + \mu \frac{\partial^2 u}{\partial z^2} = 0 \tag{1}$$

$$-\frac{\partial P}{\partial z} - \rho_m g = 0 \tag{2}$$

where P is pressure, ρ_m is magma density, g gravity, u horizontal velocity and μ viscosity. The viscosity is considered constant. In reality, magma viscosity is temperature dependent, and, as the intrusion spreads and cooling proceeds, the flow viscosity increases. Cooling, and hence the viscosity increase, do not proceed homogeneously within the flow and this might also influence the dynamics of the flow. In this model, the viscosity μ is thus an effective viscosity for the whole intrusion, for the duration of the flow [*Griffiths*, 2000]. Intrusion cooling and its effects on flow dynamics are discussed in section 6.5.

3.1.2. Pressure

[15] As in the gravity current theory, the pressure gradient across the layer is hydrostatic (2) and is easily integrated:

$$P = -\rho_m g z + P_{z=0} \tag{3}$$

At the base of the flow, the pressure $P_{z=0}$ is the sum of the hydrostatic pressure P_h due to the weight of both the magma and crust, and the elastic pressure P_e, due to the deformation of the elastic crust. The hydrostatic pressure at $z = 0$ is given by, with ρ_r the crust density:

$$P_h = \rho_m g h + \rho_r g d + P_a \tag{4}$$

where P_a is the atmospheric pressure. In the absence of horizontal forces within the elastic plate, the elastic pressure

required for bending the plate is given by the force per unit area that is necessary for a vertical displacement h of the thin elastic plate [*Turcotte and Schubert*, 1982]:

$$P_e = D\frac{\partial^4 h}{\partial x^4} \tag{5}$$

where $D = Ed^3/12\,(1-\nu^2)$ is the flexural rigidity of the plate which represents the resistance to bending of the plate; D depends on the crust elastic thickness d, Young's modulus E and Poisson's ratio ν. The total pressure at height z within the magma is thus given by

$$P = P_a + \rho_r g d + \rho_m g(h-z) + D\frac{\partial^4 h}{\partial x^4} \tag{6}$$

3.1.3. Horizontal Velocity

[16] Boundary conditions are such that the horizontal velocity u is equal to zero at both $z = h$ and $z = 0$. Using (6) in (1) and integrating twice, I obtain the following expression for u:

$$u(x,z,t) = \frac{1}{2\mu}\left(z^2 - hz\right)\left(D\frac{\partial^5 h}{\partial x^5} + \rho_m g\frac{\partial h}{\partial x}\right) \tag{7}$$

[17] Because magma spreads along a weak bedding plane, no fracture criterion is here considered. However, *Lister and Kerr* [1991] have shown that the pressure necessary for fracture extension is negligible in comparison with the elastic pressure in the case of sill propagation. In Appendix C, I also show a posteriori that the conditions for failure are met in the cases considered.

3.1.4. Mass Conservation

[18] The flow is assumed to be incompressible although, at shallow depth, the magma may contain a non-negligible fraction of gas. With this assumption, conservation of mass integrated over the intrusion thickness gives

$$\frac{\partial h}{\partial t} = -\frac{\partial}{\partial x}\int_0^h u(x,z,t)dz + w(x,t) \tag{8}$$

where w is the influx of magma into the intrusion, i.e., magma vertical velocity within the feeder dike (Figure 1).

[19] The effective overpressure ΔP^* driving the flow in the feeder conduit decreases as the intrusion thickens and is given by

$$\Delta P^*(t) = \Delta P_c - \rho_m g h_0(t) \tag{9}$$

where $h_0(t)$ is the maximum intrusion thickness at $x = 0$, $\rho_m g h_0$ is the intrusion weight at the origin and ΔP_c is the initial driving pressure or the overpressure at the base of the dike ($z = -Z_c$).

[20] In (9), the elastic pressure term $D(\frac{\partial^4 h}{\partial x^4})_{x=0}$ has been neglected. This term scales as Dh_0/l_d^4; it is thus maximum when the intrusion initiates the flow length, l_d is then minimum, and decreases with time to become negligible as l_d increases. This term represents the elastic pressure to overcome in order to initiate the flow, it vanishes as long as the flow spreads. This model assumes a large aspect ratio for the intrusion and does not consider the initiation of a lateral intrusion, where the vertical flow transitions to horizontal. On the contrary, the intrusion weight at the center $\rho_m g h_0$ is equal to zero at the beginning and increases with time.

[21] The total injection rate is thus given by

$$\frac{dV}{dt} = Q_0\left(1 - \frac{\rho_m g h_0(t)}{\Delta P_c}\right) \tag{10}$$

where Q_0 is the injection rate in case of a constant driving pressure ΔP_c. Within the feeder conduit, Poiseuille flow applies, Q_0 and the vertical velocity w are related to dike and magma properties through

$$Q_0 = \frac{\Delta P_c a^3}{12\mu Z_c} \tag{11}$$

$$w(x,t) = \begin{cases} \frac{\Delta P^*}{2\mu Z_c}\left(\frac{a^2}{4} - x^2\right) & \text{if } x \le a/2 \\ 0 & \text{if } x > a/2 \end{cases} \tag{12}$$

[22] The equation for the intrusion thickness evolution h in cartesian coordinates is then obtained using (7) in (8):

$$\frac{\partial h}{\partial t} = \frac{1}{12\mu}\frac{\partial}{\partial x}\left(\rho_m g h^3\frac{\partial h}{\partial x} + \frac{Ed^3}{12(1-\nu^2)}h^3\frac{\partial^5 h}{\partial x^5}\right) + w(x,t) \tag{13}$$

This evolution equation for the flow thickness is composed of three different terms on the right hand side. The first term represents gravitational spreading of the flow: except for a constant arising from a no-slip boundary condition at the intrusion roof, this term is the same as for a gravity current [*Huppert*, 1982]. The second term on the right represents the squeezing of the flow due to the elastic response of the crust. Both terms are negative and induce spreading. The last term represents magma injection and is positive.

3.2. Nondimensionalization

[23] Equations (13) and (10) are nondimensionalized using a horizontal scale Λ, a vertical scale H, and a time scale τ given by

$$\Lambda = \left(\frac{Ed^3}{12(1-\nu^2)\rho_m g}\right)^{1/4} \tag{14}$$

$$H = \left(\frac{12\mu Q_0}{\rho_m g}\right)^{1/4}\Lambda^{1/4} = \left(\frac{a^3\Delta P_c}{Z_c\rho_m g}\right)^{1/4}\Lambda^{1/4} \tag{15}$$

$$\tau = \left(\frac{12\mu}{\rho_m g Q_0^3}\right)^{1/4}\Lambda^{5/4} = \frac{12\mu}{(\rho_m g)^{1/4}}\left(\frac{Z_c}{a^3\Delta P_c}\right)^{3/4}\Lambda^{5/4} \tag{16}$$

where scales are chosen such that $Q_0 = \frac{H\Lambda}{\tau}$. These characteristic scales are defined by equating the nondimensional groups in front of the gravity current and elastic terms to 1, i.e., such that $\frac{\tau H^3\rho_m g}{12\mu\Lambda^2} = \frac{\tau H^3 D}{12\mu\Lambda^6} = 1$. The length scale Λ (14) is the flexural wavelength or flexural parameter as defined by *Turcotte and Schubert* [1982], i.e., the characteristic length

Table 1. Model Parameters

Parameters and Physical Properties	Symbols	Range of Values
Depth of intrusion	d	100 m–5 km
Young's Modulus	E	10–100 GPa
Poisson's ratio	ν	0.25
Gravity	g	1.62 or 9.81 m.s^{-2}
Magma density	ρ_m	2500–2900 kg/m^3
Magma viscosity	μ	10–10^{10} Pa s
feeder dike width	a	1–200 m
feeder dike height	Z_c	5–500 km
Initial overpressure	ΔP_c	5–50 MPa
Crust flexural rigidity	D	
Crust density	ρ_r	
Injection rate	Q_0	
Intrusion length scale	Λ	
Intrusion thickness scale	H	
Intrusion time scale	τ	
Maximum dimensionless thickness	h_0	
Dimensionless length	L	
Dimensional thickness	h_d	
Dimensional length	l_d	

scale over which the crust can support elastic stresses. The flexural wavelength depends primarily on the parameters characterizing the overlying elastic crust (thickness and elastic properties); it varies between 1.5 and 15 km for an elastic thickness or depth of intrusion d between 500 and 5000 m and E between 10 and 100 GPa (see Table 1 for model parameters and their ranges of values). The thickness scale (15) represents the thickness for which the gravity current and the elastic terms are of similar importance; it depends primarily on the injection rate and magma physical properties (weight and viscosity). The time scale (16) is the characteristic time to fill up a laccolith and is mainly a function of the injection rate or of magma viscosity and dike width a.

[24] Two dimensionless parameters, γ and σ, are defined:

$$\gamma = \frac{a}{\Lambda} \tag{17}$$

$$\sigma = \frac{\Delta P_c}{\rho_m g H} = \left(\frac{\Delta P_c}{\rho_m g a}\right)^{3/4} \left(\frac{Z_c}{\Lambda}\right)^{1/4} \tag{18}$$

The number γ is the normalized source width and represents the effect of the dike width a, whereas σ is the normalized pressure head, i.e., the rate between the overpressure in the reservoir below and the weight of a characteristic thickness H of magma.

[25] The dimensionless equations for the thickness and volume are then, for $|x| \leq \gamma/2$:

$$\frac{\partial h}{\partial t} = \frac{\partial}{\partial x}\left(h^3 \frac{\partial h}{\partial x} + h^3 \frac{\partial^5 h}{\partial x^5}\right) + \frac{6}{\gamma}\left(\frac{1}{4} - \frac{x^2}{\gamma^2}\right)\left(1 - \frac{h_0}{\sigma}\right) \tag{19}$$

$$\frac{dV}{dt} = \left(1 - \frac{h_0}{\sigma}\right) \tag{20}$$

For $|x| > \gamma/2$, the last term on the right-hand side of (19), i.e., the source term, is replaced by zero. The sixth spatial derivative of h in (19) causes classical numerical method used for gravity currents to be unstable. This equation is thus solved with a spectral method along a grid of finite length. More details are given in Appendix A.

3.3. Range of Values for the Dimensionless Numbers

[26] For a Young's modulus value between 10 and 100 GPa, a depth of injection between 100 and 5000 m and a gravity g = 9.81 or 1.62 m.s^{-2}, the characteristic length Λ, given by (14), varies between several hundred meters and 20 km. For a dike width between 1 and 200 m, values for $\gamma = a/\Lambda$ range between ~10^{-3} and 0.2.

[27] In terrestrial settings, the overpressure in magma reservoirs driving dike and conduit flows is typically between a few to several tens of MPa [*Barmin et al.*, 2002; *Stasiuk et al.*, 1993; *Tait et al.*, 1989]. Conduit or dike lengths Z_c are typically several kilometers and are not likely to exceed several tens of kilometers. Hence, for terrestrial settings, values for σ are in the range 1 to 100.

[28] In lunar settings, the magma probably comes from much deeper, up to a depth of several hundreds of kilometers [*Shearer et al.*, 2006]. Lunar magmas were probably drier than terrestrial ones and gas pressure buildup is probably negligible at several kilometer depth. Thus, magma buoyancy is the most likely cause of overpressure [*Wieczorek et al.*, 2001]. The parameter σ can thus be reduced to: $\sigma = \left(\frac{\Delta\rho Z_c}{\rho_m a}\right)^{3/4}\left(\frac{Z_c}{\Lambda}\right)^{1/4}$. For $\Delta\rho$ = 50 kg.m^{-3} and Z_c up to 500 km, σ may be as high as 10^3.

3.4. Scaling Analysis

[29] I develop a simple scaling analysis of (19) for the maximum flow thickness h_s in which derivatives in x are approximated by $1/L_s$, where subscript s stands for scale. This type of analysis is suitable for behavior close to the flow center x = 0 [*Michaut and Bercovici*, 2009] and is used to compare the strength of the different terms of (19). Equation (19) becomes

$$\frac{dh_s}{dt} \approx -\frac{h_s^4}{L_s^2} - \frac{h_s^4}{L_s^6} + \frac{3}{2\gamma}\left(1 - \frac{h_s}{\sigma}\right) \tag{21}$$

$$\frac{dV_s}{dt} \approx 1 - \frac{h_s}{\sigma} \tag{22}$$

[30] The gravity current term (first term on the right of (19) and (21)) becomes dominant over the elastic term (second term on the right of (19) and (21)) when

$$\frac{h_s^4}{L_s^2} > \frac{h_s^4}{L_s^6} \Rightarrow L_s > 1 \tag{23}$$

This scaling analysis predicts thus that the uplift and spreading is first controlled by the elastic response of the crust and then by the own weight of the current. Hence, a "gravity current" regime follows an "elastic regime" when the dimensionless length of the flow is of order 1.

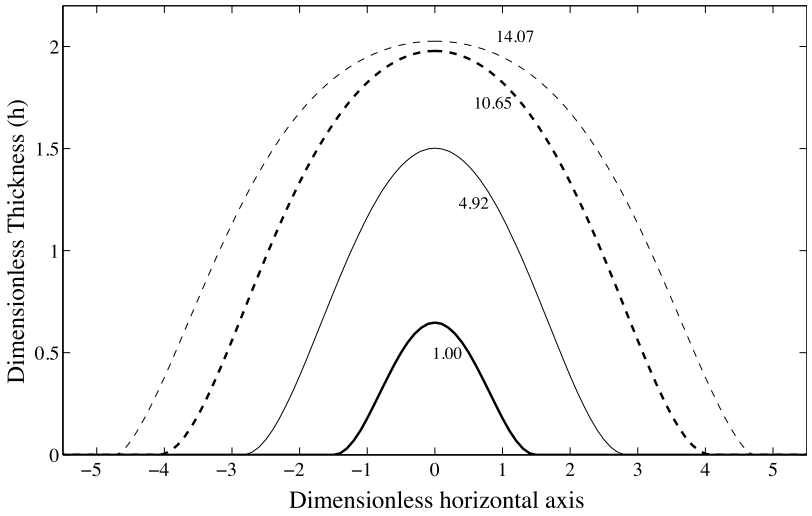

Figure 2. Shape of the flow, i.e., thickness as a function of horizontal coordinate, at four different times indicated on the graph. Variables are dimensionless, and one needs to multiply by the characteristic scales (thickness, length, or time given by (15)), (14), and (16)) to obtain the dimensional values ($\gamma = 0.25$, $\sigma = 10$).

[31] When $h_s \rightarrow \sigma$, the source term (third term on the right of (19) and (21)) goes to zero as the intrusion weight at the center compensates for the overpressure driving the flow; hence h_s cannot be larger than σ. As $h_s \rightarrow \sigma$, a third spreading regime is reached where the maximum thickness remains constant.

4. Results

[32] Numerical results show three spreading regimes: an elastic regime, a gravity current regime and a regime of lateral propagation that are described in this section and in section 5. Calculations show that the flow shape, thickness at the center and length depend only on the normalized pressure head σ, the normalized source size γ has no effect on the dynamics and shape of the flow (see Appendix A).

4.1. Flow Shape as a Function of Time

[33] Initially, as the intrusion grows with injection of more magma, the flow is self-similar and both the flow thickness and length increase with time (Figure 2). As t becomes larger than ~10, $h \sim 2$ and $L \sim 4$, the thickness of the flow does not increase as much as in the first phase and the shape of the flow changes: the intrusion inflates on the sides and the intrusion fronts become steeper. This transition reflects the change in the spreading and growth regime, when the gravity current term becomes dominant over the elastic one.

4.2. Effect of the Normalized Pressure Head σ

[34] During the first phase where the elastic term is dominant, the effect of σ on the thickness evolution is negligible (Figure 3): for different values of σ, all calculations form a single line of slope 5/9 (in logarithmic scale), predicting that $h_0 \propto t^{5/9}$ during this regime. This first phase ends when the thickness is close to ~2 and the time reaches ~10 (Figure 3). This change in the spreading regime corresponds to the change in flow morphology described in section 4.1.

[35] When h_0 reaches the value σ, the intrusion weight at the center compensates for the overpressure driving the flow and the thickness at the center remains constant (Figure 3) while the flow propagates laterally.

[36] For $t > 10$, the thickness increases much more slowly with time (i.e., with a smaller slope in logarithmic scale, Figure 3), even if the flow is not in the laterally propagating solution (as in the case for $\sigma = 10$).

[37] The evolution of the dimensionless thickness h_0 as a function of length L also shows the same behavior with different spreading regimes (Figure 4). The first elastic phase does not depend on the value of σ and is characterized by a slope larger than 1. During the second phase, the increase in thickness is much slower, and the flow grows mostly laterally. When $h_0 \rightarrow \sigma$, the regime of lateral propagation is reached as $L \rightarrow \infty$.

[38] In section 5, scaling laws are proposed for the evolution of the thickness at the intrusion center as a function of time and length.

5. Three Regimes: Characteristics and Scaling Laws

5.1. Elastic Regime

5.1.1. Scaling Laws in the Elastic Regime

[39] When both h and L are less than 1, the elastic term (second term on the right side of (19)) is dominant over the gravity current term (first term on the right side of (19)).

[40] As long as $h_0 \ll \sigma$, the overpressure ΔP_c in the reservoir below is much larger than the weight of the intrusion $\rho_m g h_0$, and the injection rate can be considered constant. If the injection occurs through a point source at the intrusion center, (19) and (20) reduce to (in dimensionless form)

$$\frac{\partial h}{\partial t} = \frac{\partial}{\partial x}\left(h^3 \frac{\partial^5 h}{\partial x^5}\right) \tag{24}$$

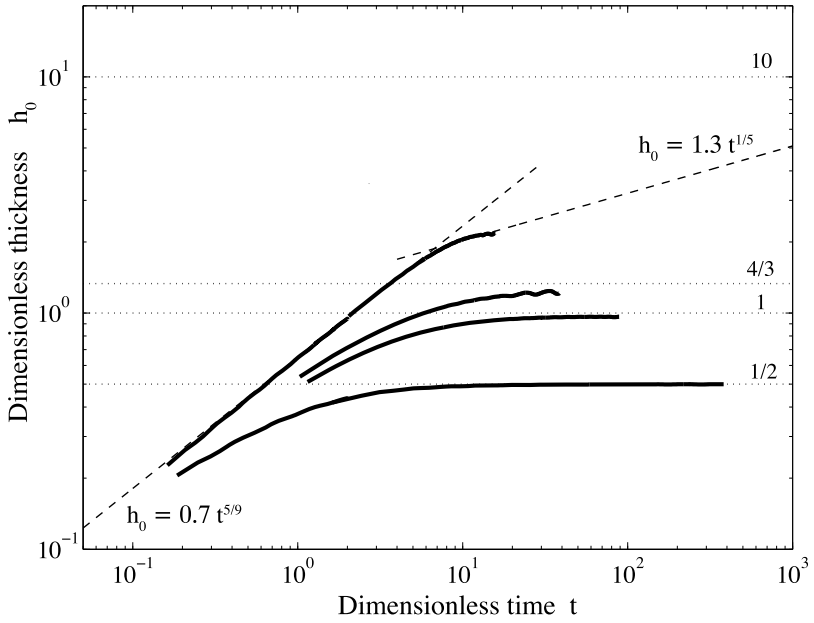

Figure 3. Maximum dimensionless thickness h_0 as a function of dimensionless time t. Bold lines, results from the numerical calculations; dashed line, $h_0 \propto t^{5/9}$ and $h_0 \propto t^{1/5}$; dotted lines, thickness at $t \rightarrow \infty$. Results are for four different values of σ: 1/2, 1, 4/3, and 10, and $\gamma = 0.25$ (although calculations do not depend on γ).

$$\int_0^{L(t)} h(x,t)dx = t \tag{25}$$

where $L(t)$ is the flow length.

[41] The variable $\eta = \frac{x}{t^\alpha}$ is introduced and I look for a similarity solution by decomposing h into

$$h(x,t) = f(\eta)t^\beta \tag{26}$$

where f and β are to be determined.

[42] Introducing (26) in (25), one finds, with η_L a constant equal to the value of η at $x = L$:

$$\int_0^{\eta_L} f(\eta)d\eta t^\beta t^\alpha = t \tag{27}$$

which gives $\beta = 1 - \alpha$. Using this result and (26) in (24) one obtains

$$t^{-\alpha}\left((1-\alpha)f - \alpha\eta\frac{df}{d\eta}\right) = t^{4-10\alpha}\frac{d}{d\eta}\left(f^3\frac{d^5f}{d\eta^5}\right) \tag{28}$$

A similarity solution exists if $t^{4-9\alpha} = 1$, i.e., $\alpha = 4/9$, which gives

$$h(\eta,t) = f(\eta)t^{5/9} \tag{29}$$

$$\Rightarrow\ L(t) = \eta_L t^{4/9} \tag{30}$$

where $f(\eta)$ characterizes the shape of the flow and is given by the solution of (28) with $\alpha = 4/9$ although no analytical solution exists for this equation.

[43] Thus, I obtain

$$h_0 \propto t^{5/9} \tag{31}$$

$$h_0 \propto L^{5/4} \tag{32}$$

These analytical solutions for the maximum thickness as a function of time (31) and length (32) and for the length as a function of time (30) closely fit the numerical results during the first spreading regime (Figures 3, 4, and 5). Numerical calculations give the value of the constants of proportionality, see Table 2.

[44] This analytical result confirms that the elastic response of the crust controls the flow during the first phase of the intrusion.

5.1.2. Shape of the Flow

[45] During the elastic regime, a simple function fits the numerical results for the shape of the flow (Figure 6):

$$\frac{h(x,t)}{h_0(t)} = \left(1 - \frac{x^2}{L(t)^2}\right)^2 \tag{33}$$

where L and h_0 are the dimensionless flow length and thickness at the center, that vary with time t.

[46] Equation (33) is the solution for the vertical displacement of a thin elastic plate of length $2L(t)$ pinned at its ends and submitted to a homogeneous pressure [*Turcotte and Schubert*, 1982]; this indicates that the viscous flow of magma due to the elastic response of the crust homogeneously distributes the available overpressure from the source over the length scale of the flow below the elastic crust. Because of the elasticity of the crust, its flexure is

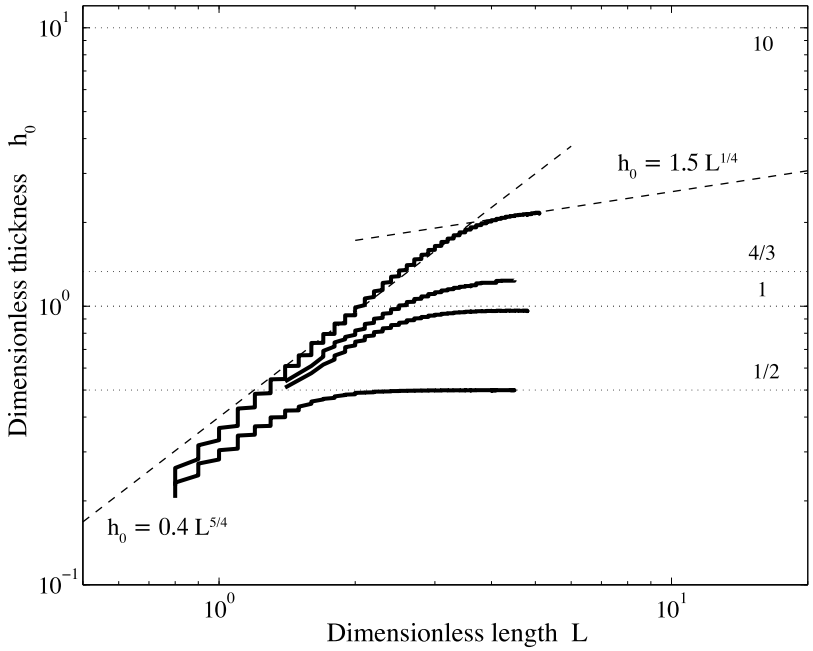

Figure 4. Maximum dimensionless thickness h_0 as a function of dimensionless length L. Bold lines, results from the numerical calculations; dashed line, $h_0 \propto L^{5/4}$ and $h_0 \propto L^{1/4}$; dotted lines, thickness at $L \rightarrow \infty$. Results are for four different values of σ: 1/2, 1, 4/3, and 10, and $\gamma = 0.25$ (although calculations do not depend on γ).

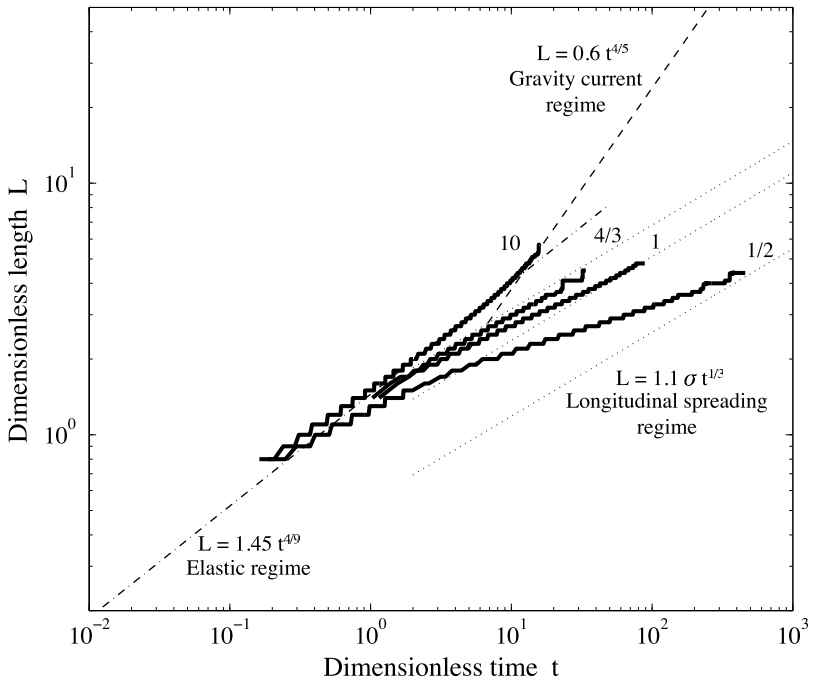

Figure 5. Flow length as a function of time from the numerical calculations (bold lines) for four different values of σ = 1/2, 1, 4/3, and 10, indicated on the graphs. Calculations are for $\gamma = 0.25$. Scaling laws obtained in the elastic (dashed-dotted line), gravity current (dashed line), and lateral propagation (dotted lines) regimes are also indicated and fit the calculations. For small values of σ = 1/2, 1, and 4/3, the transition to the laterally propagating solution is reached early and the gravity current phase is not visible.

Table 2. Scaling Laws in 2-D and Axisymmetric Geometries

Two Dimensional	Axisymmetric
Elastic Regime	
$h_0 = 0.7\ t^{5/9}$	$h_0 \propto t^{1/3}$
$L = 1.5\ t^{4/9}$	$R \propto t^{1/3}$
$h_0 = 0.4\ L^{5/4}$	$h_0 \propto R$
Gravity Current Regime	
$h_0 = 1.3\ t^{1/5}$	$h_0 = C^{te}$
$L = 0.6\ t^{4/5}$	$R \propto t^{1/2}$
$h_0 = 1.5\ L^{1/4}$	$h_0 = C^{te}$
Lateral Propagation Regime	
$L = 1.1\ \sigma\ t^{1/3}$	$R \propto \sigma^{3/4} t^{1/4}$

distributed over the whole length of the flow, i.e., over a few times the flexural wavelength Λ; and hence the shape of the flow does not depend on the normalized size of the source (parameter γ) for $\gamma \leq 1$, on the contrary to gravity currents [see *Michaut and Bercovici*, 2009].

[47] The thickness of the flow is very well fitted by a fourth-order polynomial (33), for which the elastic term is zero in (19). If (33) is only a fit and not the self-similar solution (i.e., it is not solution of (28) with $\alpha = 4/9$), it shows however that the shape of the flow is such that the elastic term is small, i.e., that in the absence of injection and gravity current terms, the flow would be very slow.

5.2. Gravity Current Regime

5.2.1. Scaling Law

[48] In this regime, the gravity current term becomes dominant over the elastic term. As long as $h_0 \ll \sigma$, the intrusion rate can still be considered constant. Therefore, the equation for a two-dimensional gravity current with constant flux applies [*Huppert*, 1982]:

$$\frac{\partial h}{\partial t} = \frac{\partial}{\partial x}\left(h^3 \frac{\partial h}{\partial x}\right) \tag{34}$$

$$\int_0^{L(t)} h(x,t)\,dx = t \tag{35}$$

The same exercise as above, and as developed by *Huppert* [1982], shows that a similarity solution to these equations exists and gives

$$h_0 \propto t^{1/5} \tag{36}$$

$$L \propto t^{4/5} \tag{37}$$

$$h_0 \propto L^{1/4} \tag{38}$$

[49] The exponents relating the thickness to the length and time are both much smaller than 1, showing that the uplift is much slower during the gravity current regime than during the elastic regime. Scaling laws in the gravity current regime for the thickness at the intrusion center as a function of time (36) and length (38) as well as for the length as a function of time (37) are in good agreement with the numerical results (Figures 3, 4, and 5 for $\sigma = 10$). Numerical calculations give the value of the constants of proportionality (see Table 2).

5.2.2. Shape of the Flow

[50] During the gravity current regime, the normalized shape of the flow develops steeper fronts (Figure 6). Steep

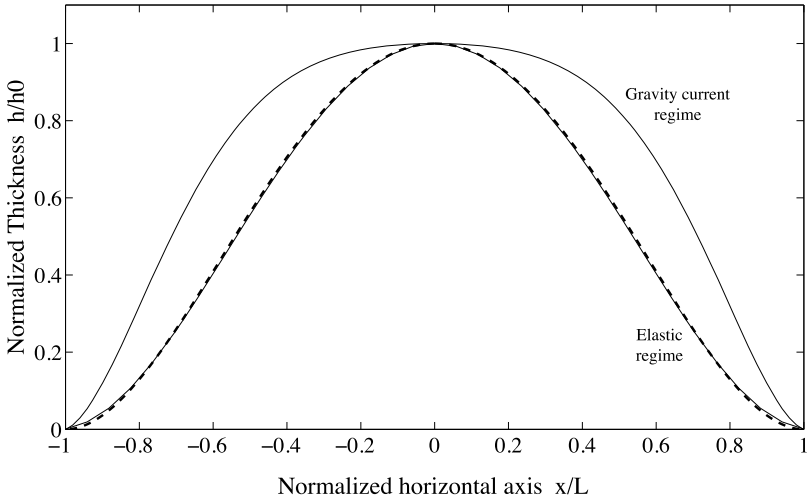

Figure 6. Characteristic shape of the intrusion in the elastic and in the gravity current regime: flow thickness normalized by the maximum thickness as a function of horizontal axis normalized by flow length. Solid lines, results from the numerical calculations in the elastic and gravity current regime; dashed line, shape given by (33). During the elastic regime the flow shape remains undistinguishable from (33); during the gravity current regime the shape progressively evolves from (33) toward a shape with steeper edges.

fronts are characteristics of gravity currents [*Huppert*, 1982]. At the intrusion roof, the curvature becomes important toward the tip where the resistance to bending (5), and hence the elastic response of the crust, become non-negligible. Gravity currents show a vertical slope at their fronts but in this case, the elastic deformation of the crust always imposes a zero derivative of the flow thickness h at the tip. Hence the gravity current shape is never completely reached. In this case also the shape of the flow does not depend on γ.

5.3. Lateral Propagation

[51] Once $h_0 \rightarrow \sigma$, the flow is thick enough to accommodate the overpressure below. The thickness at the center remains constant and the flow enters the regime of lateral propagation, where only its length increases. In this regime, the elastic term is negligible. However, this term ensures that the magma overpressure is homogeneously distributed over a length scale of the order of the characteristic length of the flow Λ (see section 5.1.2), which is equivalent to $\gamma \sim 1$. Using these assumptions with $\gamma = 1$, scaling analysis of (19) gives

$$\frac{dh_s}{dt} = -\frac{h_s^4}{L_s^2} + \frac{3}{2}\left(1 - \frac{h_s}{\sigma}\right) = 0 \tag{39}$$

where, as in section 3.4, derivatives by x are approximated by $1/L_s$ and subscript s denotes the scales. The shape of the flow is approximated to a rectangle, hence $V_s \sim h_s L_s$, and, using $h_s \sim \sigma$ and (20), one obtains

$$\frac{h_s^4}{L_s^2} = \frac{3}{2}\left(1 - \frac{h_s}{\sigma}\right) = \frac{3}{2} h_s \frac{dL_s}{dt} \tag{40}$$

$$\Rightarrow L_s^2 \frac{dL_s}{dt} = 2/3\sigma^3 \tag{41}$$

$$\Rightarrow L_s \propto \sigma (2t)^{1/3} \tag{42}$$

Numerical calculations for $\sigma = 0.5$, 1 and 4/3 show indeed that the dimensionless length L goes as $\sigma\, t^{1/3}$ once the lateral propagation regime is reached (Figure 5).

5.4. Summary of the Results

[52] The characteristic length of a viscous flow below an elastic crust is controlled by the resistance to bending of the crust (the flexural wavelength). However, the characteristic thickness of the flow mostly depends on the injection rate and magma physical properties, i.e., magma weight and viscosity, an aspect which has been neglected in previous models related to laccolith growth in particular.

[53] In a first stage, intrusion growth is dominated by the flow of magma due to the elastic deformation of the overlying crust and the intrusion keeps a self-similar shape as it grows. In two-dimensional geometry, the dimensionless shape of the flow is well approximated by (33) (Figure 6); together with the dimensionless relation $h_0 = 0.4\ L^{5/4}$ (Figure 4) and (15) this expression gives the dimensional shape of the flow as a function of x:

$$h_d(x) = 0.4\ l_d^{5/4} \Lambda^{-1} \left(\frac{a^3 \Delta P_c}{\rho_m g Z_c}\right)^{1/4} \left(1 - \frac{x^2}{l_d^2}\right)^2 \tag{43}$$

where h_d and l_d are the dimensional thickness and length of the flow, x is also dimensional and Λ is given by (14). During the elastic regime, the relatively large value of the power law exponent relating the flow thickness to length (equal to 1 in the axisymmetric case, see Appendix B, and 1.25 in the two-dimensional case) suggests that uplift and spreading occurs simultaneously.

[54] In the two-dimensional case, the transition to the gravity current regime occurs when the intrusion length and thickness become larger than $\sim 2H$ and $\sim 4\Lambda$, respectively (Figure 7), and when the time becomes larger than $\sim 10\tau$ (Figure 3).

[55] During the gravitational spreading regime, the intrusion mainly experiences lateral spreading as the uplift is negligible or very slow, with an exponent relating flow thickness to flow length equal to 0 in the axisymmetric case and 0.25 in the two-dimensional case (Figure 7) [*Huppert*, 1982]. The intrusion shape develops steeper fronts which induces thickening on the intrusion sides (Figure 6), although the elastic deformation of the crust always ensures a progressive decrease of the thickness at the front.

[56] When the thickness reaches $h_{d\infty} = \Delta P_c/\rho_m g$, it remains constant and the flow enters a third regime of lateral propagation where the flow length increases as $\sigma t^{1/3}$ in the two-dimensional case and as $\sigma^{3/4} t^{1/4}$ in the axisymmetric case (see Appendix B).

6. Discussion

6.1. Intrusion Shape and Thickness

[57] Laccolith shapes are usually modeled by the upward deflection of an overlying elastic strata due to a given magma pressure $\bar{P}$ using the a priori assumption that the width of the laccolith is fixed [*Pollard and Johnson*, 1973; *Turcotte and Schubert*, 1982]. In this theory, the magma pressure $\bar{P}$ available for lifting the plate is a free parameter and it cannot be related to any pressure-related physical parameters such as the driving pressure for the flow or magma weight. Using plate bending theory, the thickness of the laccolith in 2-D under constant magma pressure $\bar{P}$ is given by

$$h_d(x) = \frac{\bar{P}}{24D} l_d^4 \left(1 - \frac{x^2}{l_d^2}\right)^2 \tag{44}$$

[58] However, laccolith width evolves as the intrusion grows. *Kerr and Pollard* [1998] propose a treatment of laccolith evolution but prescribe a horizontal pressure distribution in the magma. In the model presented here, the shape, length and thickness of the flow evolve with time, and flow length and horizontal pressure distribution within the flow are self-consistently determined. The dimensional thickness of the flow as a function of dimensional length is, however, well described by (43). Equation (43) corresponds to (44) but where the magma pressure $\bar{P}$ depends on the

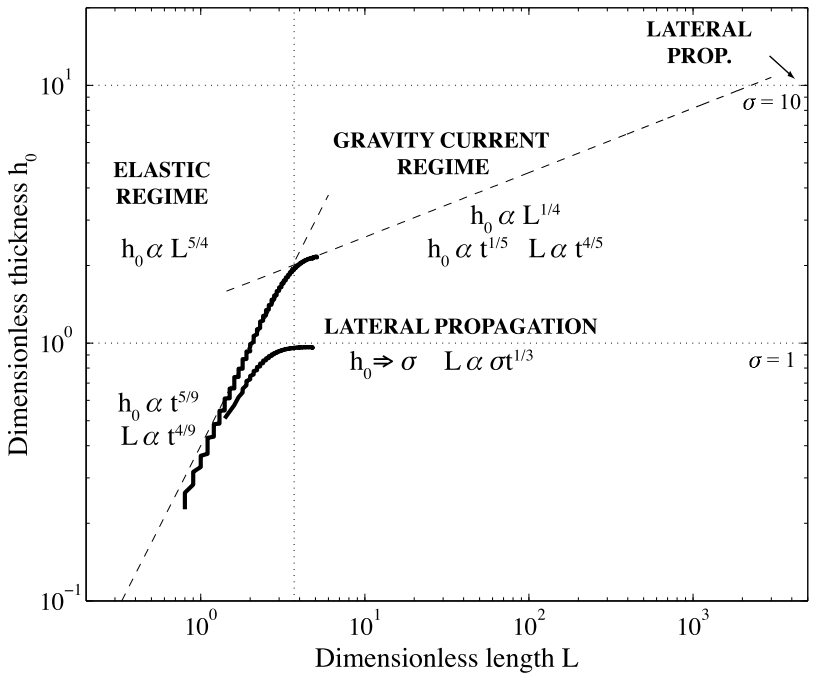

Figure 7. The dynamics of a magmatic intrusion spreading below an elastic crust shows three spreading regimes: elastic, gravity current, and lateral propagation, that are characterized by different scaling laws and dimensions (length and thickness).

length scales of the flow as well as on the overpressure in the feeder dike:

$$\bar{P} = 24 \times 0.4 \left(\frac{\Lambda}{l_d}\right)^{11/4} \left(\frac{\Delta P_c \Lambda}{Z_c}\right)^{1/4} (\rho_m g a)^{3/4} \qquad (45)$$

$$\bar{P} = 24 \times 0.4 \left(\frac{\Lambda}{l_d}\right)^{11/4} (12 \mu Q_0 \Lambda)^{1/4} (\rho_m g)^{3/4} \qquad (46)$$

where $\Lambda = (D/\rho_m g)^{1/4}$ is the flexural wavelength or parameter given by (14). Hence, this model provides insights into the magma pressure available for deforming the plate in terms of magma and crust physical properties and driving pressure or injection rate. In particular, expressions (45) and (46) show that the homogeneous pressure available for deforming the elastic plate increases with the injection rate and in particular with the dike width and pressure gradient driving the flow; it decreases as the flow spreads and l_d increases, as the available overpressure is then distributed over a larger width.

[59] From (43) the dimensional thickness h_{0d} at the center of the intrusion in the elastic regime is

$$h_{0d} = 0.4\, l_d^{5/4} \Lambda^{-1} \left(\frac{a^3 \Delta P_c}{\rho_m g Z_c}\right)^{1/4} = 0.4 \left(\frac{l_d}{\Lambda}\right)^{5/4} H \qquad (47)$$

The intrusion thickness depends thus on the crust elastic properties but also on magma physical properties and injection rate, aspects that were not considered in the previous models on laccolith shape [*Pollard and Johnson*, 1973; *Turcotte and Schubert*, 1982].

[60] In the gravity current regime, the flow thickness does not increase much more. Hence this expression can be compared to the maximum thickness of intrusions. The flexural wavelength Λ does not depend on magma physical properties and, in the elastic regime, $l_d \leq 4\,\Lambda$. However, both the dike width a and overpressure gradient $\Delta P_c/Z_c$ tend to increase as magma composition becomes more evolved and viscosity increases. Indeed, observations and physical analysis show that mafic magmas with low viscosities ($\sim 10^1$–10^2 Pa s) form dikes about 1 m wide whereas felsic magmas, with viscosities $\sim 10^6$–10^7 Pa s, form dikes of the order of several tens of meters to 100 m wide [*Bruce and Huppert*, 1989; *Wada*, 1994; *Kerr and Lister*, 1995].

[61] Using an overpressure gradient 1 order of magnitude larger and a dike width 2 orders of magnitude larger for a felsic intrusion (relative to a mafic one) leads to a maximum thickness ~56 times larger for the felsic intrusion. This model thus implies that, in the upper crust, felsic intrusions tend to form laccoliths with a maximum thickness of a few hundred meters, while mafic magmas tend to form thin elongated intrusions less than ~10 m thick, in agreement with observations.

[62] Intrusion shapes develop steeper fronts when they reach the gravity current regime. Hence, one should be able to differentiate between an intrusion that has reached the gravity current regime from one which has stopped in the elastic one from their shapes. However, this consideration might be complicated by the fact that magma viscosity is not constant, as assumed here, but temperature dependent; and this will also play in the same way, i.e., induces steeper fronts (see section 6.4) in both regimes. Another way of distinguishing a gravity current type intrusion from an elastic one is to estimate its characteristic length Λ and to compare with the intrusion length l_d. If l_d is larger than ~4Λ, then the intrusion is likely to have reached the gravity current regime.

Table 3. Dimensional Parameters of the Intrusive Layers at Elba Island, Italy, From *Rocchi et al.* [2002]

Unit	Layer	Thickness (m)	Length (km)	Depth (km)
		Central Elba		
Flysch (Complex V), San Martino	layer 3	700	8.3	1.9
Flysch (Complex V), San Martino	layer 2	100	2.4	2.0
Flysch (Complex V), San Martino	layer 1	200	5.0	2.2
Flysch (Complex V), Portoferraio	layer 4	400	10	2.6
Capo Bianco	layer 2	≥120	3.5	2.6
		Western Elba		
Hornfels (Complex IV), Portoferraio	layer 3	700	9.3	3.1
Capo Bianco	layer 1	50	1.6	3.0
Ophiolite (Complex IV), Portoferraio	layer 2	280	≥1.9	3.3
Ophiolite (Complex IV), Portoferraio	layer 1	210	≥2.5	3.7

6.2. Scaling Laws for Laccolith Morphology

[63] *Rocchi et al.* [2002] studied a series of 9 laccolith layers at Elba Island, Italy, and found a characteristic power law relationship linking intrusion thickness T and length L_d that differs from the general power law relationship of *McCaffrey and Petford* [1997], with an exponent larger than 1, which is interpreted as reflecting the record of vertical inflation stage in laccolith growth:

$$T = 0.026 L_d^{1.36} \tag{48}$$

[64] *Rocchi et al.* [2002] provide data for the intrusion depths (see Table 3), which are different for each laccolith layer. Using these depths and characteristic values for various properties of the system (see Figure 8), the length and thickness scales can be estimated for each laccolith such that the data can be nondimensionalized. For this example, each laccolith is part of a larger intrusive system, and hence variability of the model parameters should be limited, except for the elastic crust thickness, taken to be the intrusion depth, whose variation between laccoliths is accounted for in the nondimensionalization. In this case, the best fit for the dimensionless thickness h_0 is proportional to $L^{1.25}$, in very good agreement with the elastic scaling law in two dimensions (32) (Figure 8). The dimensionless intrusion lengths are smaller than 4, also supporting a flow in the elastic regime for all intrusions. The geometry of these laccoliths is not well known and probably not perfectly two-dimensional or circular but *Rocchi et al.* [2002] observe that laccolith layers are connected by feeder dikes, the major one being ~1.5 km long, indicating a 2-D contribution.

[65] Therefore, application of the model to terrestrial data shows that laccolith morphologies are well explained by the elastic spreading regime.

[66] The power law relationship $T = 0.12\ L_d^{0.88}$ proposed by *McCaffrey and Petford* [1997], shows an exponent close to 1 but smaller. The difference in exponents between this relation and the elastic scaling law in axisymmetric or even 2-D geometry might result from fitting dimensional data with a scaling law, since data should first be nondimensionalized to account for intrinsic scales of different settings. An exponent smaller than 1 would also result from fitting all the data with a single scaling law; however at least two scaling laws, characterizing two different spreading regimes (elastic and gravity current), may be required.

[67] The assumptions of the model are such that they restrain its applicability to intrusions that have already initiated and are sufficiently long that the conditions of thin elastic plate and small aspect ratio are met. The thin elastic plate condition is probably the most restrictive, hence, flow length must be at least of the order of the plate thickness for the model to be applicable, i.e., larger than several hundreds of meters to about a kilometer long. This model provides however interesting insights into the mechanism of laccolith formation. In particular, the power law relation between thickness and length is well explained by viscous magma flow below an elastic crust. Furthermore, this model sug-

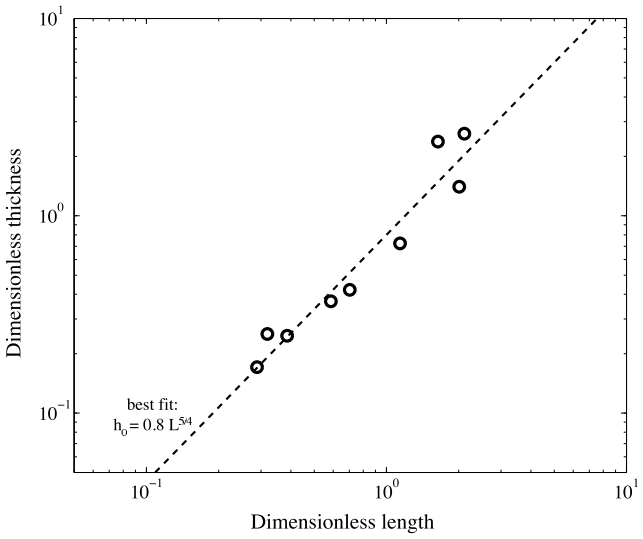

Figure 8. Dimensionless maximum thickness h_0 as a function of dimensionless half-length for laccolith layers from Elba Island, Italy. Thickness, length and depth of intrusions, or elastic crust thickness d are taken from *Rocchi et al.* [2002]. In the model the flow length is the length from the intrusion center to the front (Figure 1); the lengths provided by *Rocchi et al.* [2002] are the total intrusion lengths, which are thus divided by 2 for comparison with the model. Other parameters used for calculating H and Λ from (15) and (14) are a = 150 m, E = 10 GPa, ν = 0.25, ρ_m = 2600 kg.m^{-3}, ΔP_c = 50 MPa, Z_c = 5 km, and g = 9.81 m.s^{-2}. For depth of intrusions between 1.9 and 3.7 km, H is between 260 and 300 m and Λ is between 4 and 6.5 km. Dashed line, $h_0 \propto L^{5/4}$ as for the elastic scaling law.

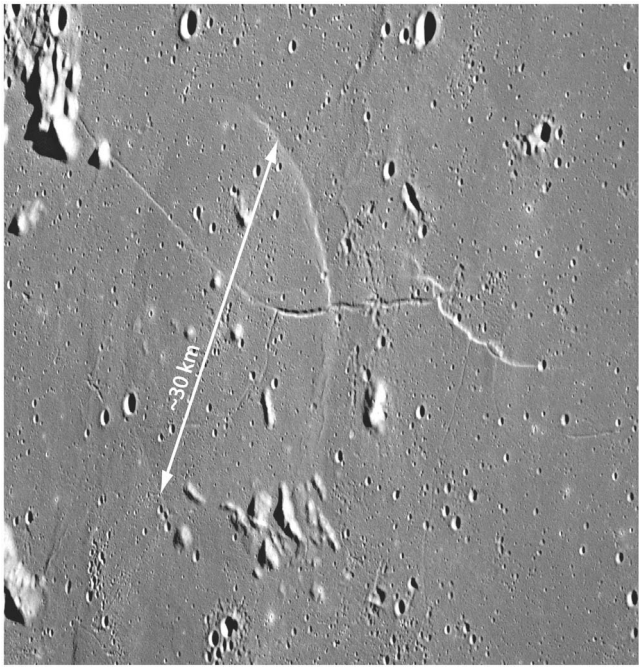

Figure 9. Apollo 15 orbital image AS15-91-12372, oblique view of the Valentine dome. The diameter of this dome is ~30 km in average.

gests that the main phase of laccolith growth and spreading does not require a two-stage process, with horizontal spreading of a sill followed by vertical inflation, as often proposed [*Johnson and Pollard*, 1973; *Corry*, 1988], or by sill stacking [*Menand*, 2008], but that spreading and inflation occur simultaneously.

6.3. Low-Slope Domes on the Moon

[68] On the Moon, thirteen elongated low-slope domes have recently been identified as possibly formed by laccolith-type intrusions [*Wöhler et al.*, 2009, 2010], although their diameters are larger and their thicknesses smaller than most terrestrial laccoliths: for a given intrusion thickness, lunar low-slope domes are at least twice as wide as terrestrial laccoliths (Figure 10a). Because these domes are subtle structures with low elevation and low slopes, the determination of their morphometric properties is complex; *Wöhler et al.* [2009] used an image-based 3-D reconstruction approach which relies on a combination of photoclinometry and shape from shading techniques. The error in the determination of the dome height is the largest one and amounts to 10% [*Wöhler et al.*, 2006]. The Valentine dome is one of the largest of these domes (Figure 9); it has an elliptical shape, i.e., a structure in between 2-D and cylindrical. These candidate intrusive domes are located in regions of extensive effusive activity, in general near the borders of Mare basalts.

[69] Using (14) and (15), both the characteristic length and thickness can be calculated in lunar versus terrestrial settings. On the Moon, the smaller gravity (g = 1.62 m.s^{-2} versus 9.81 m.s^{-2} for the Earth) leads to a characteristic length for intrusions 1.6 times larger than on Earth, i.e., close to twice as long as terrestrial ones, as observed by *Wöhler et al.* [2009]. For instance, using a Young's modulus E = 10 GPa and an intrusion depth of 1500 m, the characteristic length for lunar intrusions is ~5 km but it is ~3.2 km for terrestrial ones.

[70] On Earth, laccoliths are generally formed by relatively evolved lavas that may have differentiated from primitive magma in deep crustal magma chambers, located some 5 to 15 km below the surface. The overpressures driving magmatic ascent are typically 20 to 50 MPa, [*Tait et al.*, 1989; *Barmin et al.*, 2002; *Stasiuk et al.*, 1993] which gives overpressure gradients of ~ 10^4 Pa.m^{-1}.

[71] On the Moon, *Wilson and Head* [2008] show that because of the low density of the lunar crust, the overpressure gradient driving magma flow within the feeder dikes of mare basalts lies within a factor of 5 of 20 Pa.m^{-1}. Because of the smaller gravity and colder interior, the likely magma source for these intrusions is much deeper than for terrestrial laccoliths: most of the Mare basalts are thought to be a product of melting initiated deep in the lunar mantle, deeper than 400 km [*Shearer et al.*, 2006; *Elkins-Tanton et al.*, 2003]. Using the same value for the driving pressure on the Moon than on the Earth, ΔP_c = 50MPa, although lunar magmas are likely to be more mafic and contain less volatiles implying smaller driving pressure, and a depth of 500 km for the magma source region, the overpressure gradient is indeed only 100 Pa.m^{-1}.

[72] Dike width also increases with viscosity [*Wada*, 1994; *Kerr and Lister*, 1995]; *Bruce and Huppert* [1989] have shown that the critical dike width for magma propagation increases with viscosity to the power 1/4. Using a width a equal to 25 m for the feeder dike of lunar intrusions and 100 m for terrestrial felsic dikes (as well as other parameters values listed in Figure 10), a characteristic thickness for lunar laccoliths is 35 m; but is 190 m for terrestrial intrusions.

[73] The same ratio between the characteristic thicknesses of lunar and terrestrial intrusions is obtained if one considers the same rate of injection Q_0 in (15) but a viscosity value 5000 times lower for lunar magmas than for terrestrial ones.

[74] After nondimensionalization, terrestrial and lunar data nearly collapse to the same curve and the elastic scaling law of the model fits both lunar and terrestrial data in a 2-D geometry (Figure 10b) as well as in an axisymmetric geometry which requires a different nondimensionalization (see Figure 10c). Given that the same intrusion depth has been arbitrarily chosen for all intrusions, the fit is surprisingly accurate. The gravity current regime does not provide a good fit to the data (Figure 10b).

[75] This model therefore explains the difference in morphology between terrestrial laccoliths and low-slope domes on the Moon; it also suggests that lunar low-slope domes are indeed good candidates for laccolith intrusions at shallow depths.

[76] After nondimensionalization, the largest lunar domes plot at the limit between the elastic and the gravity current regimes (i.e., their dimensionless lengths are close to ~4). Hence it is possible that the largest lunar domes have reached the gravity current regime, although this would depend on their depths of intrusion. If they are indeed gravity current type intrusions, they should show steeper fronts than the smaller domes.

6.4. Intrusion Cooling

[77] This model assumes an isothermal, isoviscous flow, whereas, in reality, intrusions cool as they spread and magma viscosity is temperature dependent. Cooling leads to an important increase in viscosity which might influence flow dynamics as well as its shape. A more complex theory is necessary to study the effects of cooling; however, some conclusions can be readily derived. Cooling of the intrusion is much faster at the fronts, where the flow is thin, than at the center. Hence the magma will be more viscous at the flow fronts which can act as a plug and slow down the intrusion. *Bercovici* [1994] has shown that cooling viscous gravity currents with temperature-dependent viscosity grow more by thickening and develop steeper fronts than isoviscous ones that grow more by spreading. Thus, taking into account the temperature dependence of magma viscosity might lead to increase the thickening rate of the intrusion in the elastic as well as the gravity current regime, i.e., to larger slopes for the relationships between thickness and time and thickness and length in logarithmic scale in both regimes. An intrusion characterized by a variable viscosity might also develop steeper fronts, in all three dynamic regimes; this might partly explain why sedimentary strata are nearly horizontal and little deformed on top of laccoliths but are steeply bent over their peripheries [*Koch et al.*, 1981].

[78] The decrease in temperature induces crystallization and solidification of the intrusion, which might stop it from spreading. In a first approximation, the time scale for conductive cooling of an intrusion provides for an estimate for the characteristic time for flow solidification. As advective cooling is not negligible, this time scale is an upper limit. On Earth, the circulation of groundwater through hydrothermal systems within the crust largely participates in the cooling of shallow magmatic intrusions, which leads to even shorter time scales for the cooling of terrestrial intrusions. On the Moon, this is obviously not the case and cooling of the intrusion is limited to conduction of heat in the wall rock and conduction and advection of heat in the magma itself. Hence, this difference might also contribute to the fact that inferred lunar laccoliths spread further than terrestrial ones: after nondimensionalization, lunar intrusive domes plot on the upper part of the elastic scaling law (Figures 10b and 10c), whereas terrestrial laccoliths generally show smaller dimensionless length.

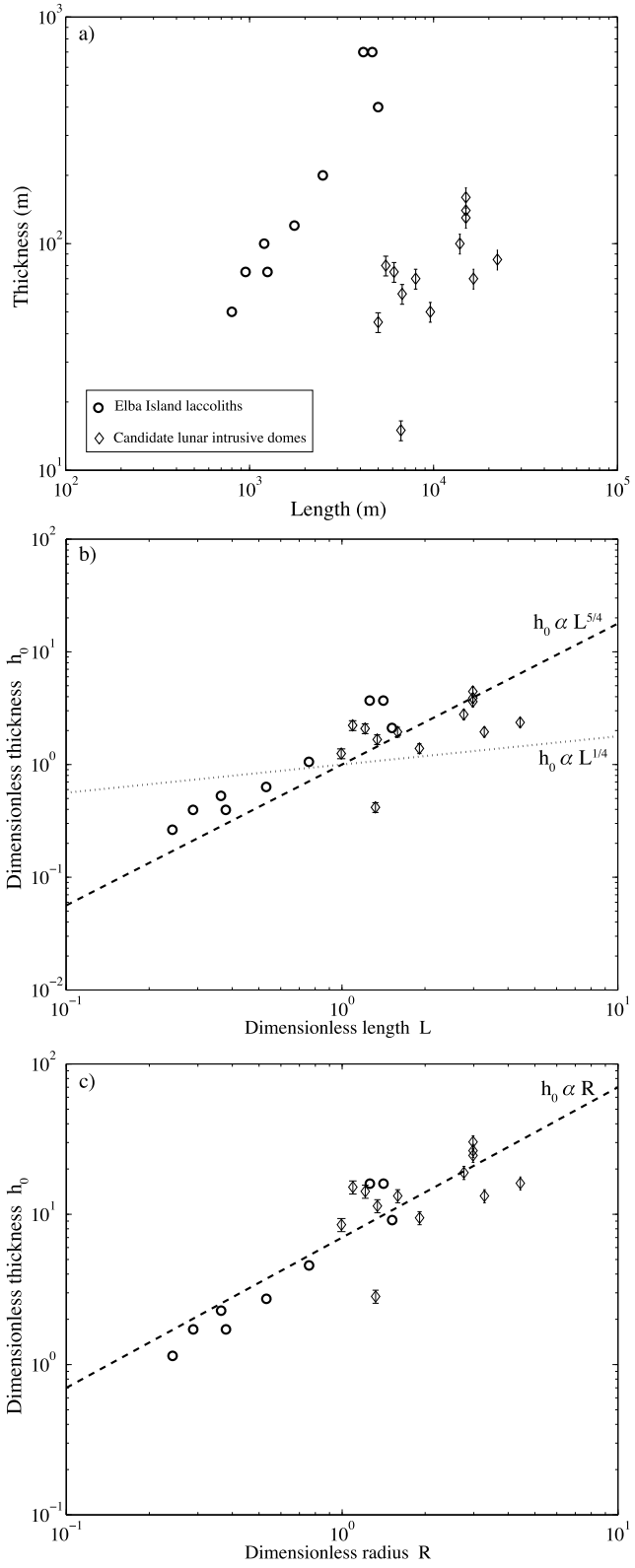

Figure 10. (a) Thickness as a function of half-length or radius for terrestrial laccoliths from Elba Island, Italy (circles) [*Rocchi et al.*, 2002], and for candidate lunar intrusive domes (diamonds) [*Wöhler et al.*, 2009]. Uncertainties for lunar dome heights amounts to 10%. (b) Dimensionless thickness as a function of dimensionless half-length or radius, characteristic thickness, and length are calculated from (15) and (14). Dashed line, 2-D elastic scaling law; dotted line, 2-D gravity current scaling law. (c) Dimensionless thickness as a function of dimensionless half-length or radius, characteristic thickness, and radius are calculated from (B8) and (B7). Dashed line, axisymmetric elastic scaling law. In both geometries, I use, for terrestrial laccoliths, g = 9.81 m.s^{-2}, $\Delta P_c/Z_c$ = 10000 Pa/m, ρ_m = 2600 kg.m^{-3}; a = 100 m, and for lunar intrusive domes, g = 1.62 m.s^{-2}, $\Delta P_c/Z_c$ = 100 Pa.m^{-1}, ρ_m = 2900 kg.m^{-3}, a = 25 m. In all cases, E = 10 GPa, d = 1500 m, ν = 0.25.

6.5. Time Scale for Laccolith Formation

[79] The transition from the elastic to the gravity current regime occurs at a time $\tau_f = 10\tau$, which provides an estimate for the time scale of laccolith formation.

[80] Using the parameters listed in Figure 10, the maximum time scale for the formation of terrestrial laccoliths τ_f is $\sim 3 \times 10^{-2} \times \mu$ (in units of seconds); it increases with Young's modulus and intrusion depth and decreases with overpressure gradient and feeder dike width (16). This time scale is about a month to 10 years for effective viscosity values of $\sim 10^8$ to 10^{10} Pa s that are representative of rather cold, crystal-rich silicic magmas. Hence this model predicts that laccolith intrusions are short geological events.

[81] One can compare the laccolith formation time with the characteristic time for conductive cooling of an intrusion τ_d given by: $\tau_d \sim \bar{h}^2/4\kappa$ for an intrusion of thickness $\bar{h}$ and a thermal diffusivity κ. The mean thickness of a laccolith is given by

$$\bar{h} = h_0 \int_0^1 \left(1 - x^2\right)^2 dx = \frac{8h_0}{15} \tag{49}$$

which gives $\bar{h} \sim 106$ m for $h_0 = 200$ m. The characteristic time for conductive cooling of an intrusion of mean thickness $\bar{h} \sim 106$ m is about 90 years, which is larger than the time scales estimated above. However, as discussed in section 6.4, this characteristic time for cooling is an upper limit as cooling by advection and by groundwater circulation on Earth are not negligible.

[82] By simulating the thermal evolution of a growing pluton and its wall rock for different construction scenarii, *Habert and de Saint-Blanquat* [2004] estimated a maximum duration of ~60 years for the emplacement of the Black Mesa intrusion, Henry Mountains, in agreement with the time scales provided by this model.

[83] In the case of lunar laccoliths, using values for the parameters listed in the caption of Figure 10, the maximum time scale for laccolith formation is $\sim 20 \times \mu$ (in units of seconds), i.e., $\sim 10^3$ times longer than terrestrial laccoliths for similar magma viscosity. The maximum thickness for lunar intrusive domes varies between 15 and 110 m, which gives average intrusion thicknesses between ~8 and 60 m using (49) and characteristic times for conductive cooling τ_d between 0.5 and 30 years. Using this range of values as upper values for the emplacement time scale, I estimate maximum magma viscosities for these candidate intrusions between $\sim 5 \times 10^5$ and 5×10^7 Pa s. These viscosity estimates, even as an upper limit, seem relatively large in comparison with the range of viscosities characteristics of basalts at the liquidus (typically 10 to 10^3 Pa s), and mare basalts in particular, which have a lower concentration in alkalies than terrestrial basalts, hence an even lower viscosity [*Shearer et al.*, 2006]. However, a decrease in water content and temperature may also contribute to increase magma viscosity. *Del Gaudio et al.* [2010] estimated a viscosity at least 2 orders of magnitude larger for an anhydrous synthetic alkaline basalt than for the same basalt containing 1.3 wt% H_2O, over a large range of temperatures, at 500 MPa. A decrease in temperature, as magma ascends and flow spreads, leads to crystallization and evolution of the residual melt composition, hence to an increase in viscosity that can be significant: *Villeneuve et al.* [2008] measured the viscosity of a natural basalt sample as a function of temperature and found that a decrease in temperature from the liquidus (~1390°C) to the glass transition (~640°C) causes an increase in viscosity from $\sim 10^1$ to 10^{10} Pa.s. Hence these large viscosity values may reflect low temperature and potentially anhydrous and crystal-rich basalt emplaced at much smaller rates than mare basalts. Furthermore, following the treatment of *Wilson and Head* [2003] to evaluate dome yield strength and viscosity, *Wöhler et al.* [2007] estimated even larger viscosity values for low-Si basaltic lunar mare domes, as high as 10^6 to 10^8 Pa s.

7. Conclusion

[84] The characteristic length of a shallow magmatic intrusion is controlled by the resistance to bending of the crust (the flexural wavelength), whereas its characteristic thickness is related to the injection rate and magma physical properties, i.e., magma weight and viscosity.

[85] The model predicts that the spreading of an intrusion is first controlled by the flexural response of the crust. As the intrusion length and thickness become larger than a characteristic length and thickness, the flow transitions to a gravity current regime. When the flow is thick enough to accommodate the pressure head, it follows a third regime of lateral propagation. The three regimes are characterized by specific scaling laws for the thickness as a function of time and length (Table 2).

[86] As expected, the intrusion shape in the elastic regime fits observed terrestrial laccolith shape, which can be modeled by the upward deflexion of a thin elastic plate under an applied magma pressure. However, this model allows to relate this rather unspecific magma pressure to laccolith geometry, crustal and magma physical properties, and more importantly, to the injection rate. The scaling law for the thickness versus length in the elastic regime also fits the observed variability in terrestrial laccolith geometry, i.e., the increase in intrusion thickness versus length, hence providing for a physical explanation for the observed relationship between laccolith length and thickness.

[87] On the Moon, the gravity is lower which would lead to a larger characteristic length for shallow lunar intrusions; the magma is also more mafic, implying a smaller characteristic thickness. Hence this model predicts that lunar laccolith will be both larger in extent and smaller in thickness than terrestrial ones. Indeed, after nondimensionalization, the geometry (dimensionless length versus thickness) of terrestrial laccoliths and inferred ones on the Moon follow the same curve which is well fitted by the elastic scaling law.

[88] Finally, this model predicts that laccolith form over relatively short time scales, i.e., less than ~100 years.

Appendix A: Numerical Calculations

[89] The sixth derivative of h with x in (19) makes the resolution of this equation problematic. Both finite differences and the finite volume method [*Patankar*, 1980], which is usually well adapted to gravity current equations [*Bercovici and Lin*, 1996; *Michaut and Bercovici*, 2009], are unstable. Consequently, equation (19) is solved with a

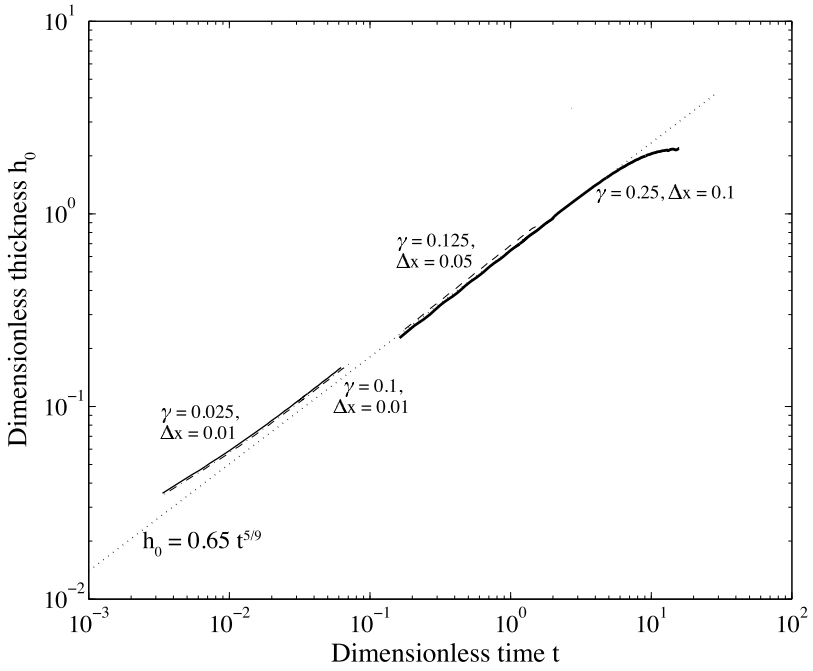

Figure A1. Evolution of the dimensionless thickness as a function of time for different values of γ and Δx indicated on the graph. Differences between calculations are negligible and come from difference in the value of Δx; γ has no effect on the results.

pseudospectral method in space (by fast Fourier transform [*Canuto et al.*, 2007]), and a semi-implicit finite difference method in time.

[90] Calculations are made along a domain of finite length of N grid points, much larger than the flow ($N = 2^{14}$). The total spatial frequency (i.e., inverse of wavelength) range for the fast Fourier transform is thus $0–1/2\Delta x$, with a sampling frequency of $1/(\Delta x N)$, Δx being the spatial step size. Numerical integration in time of this equation is also particularly onerous. Due to the sixth spatial derivative of h in (19), the time step must be extremely small, even for relatively large values of $\Delta x = 0.1$. As the energy spectra of the fast Fourier transform is concentrated over about one third of the total frequency range, aliasing is reduced by padding the fast Fourier transform with zeros for frequencies lower than $N/(4\lambda)$, where $\lambda = N\Delta x$ is the total length of the grid. With this treatment, the time step size can be increased by a factor 2^6. The time step size Δt is recalculated at each time step and has been optimized to the value

$$\Delta t = \frac{2^6 \Delta x^6}{\pi^6 h_0^3} \tag{A1}$$

The maximum thickness $h_0(t)$ increases with time, thus Δt decreases as the intrusion grows. Convergence tests verify that a decrease in the time step size does not change the results.

[91] Hence, Δx must be large enough so that Δt is not too small and the integration over a significant time range does not take too long. For the results shown in the main text, I used $\Delta x = 0.1$ and calculations start with an initial volume such that the flow maximum thickness and length are $h_0 = 0.01$ and $L = 1$, respectively; that is, the initial volume is distributed over 21 grid points. The initial shape and volume of the intrusion has no effects on the results. For $\Delta x = 0.1$, the normalized source width γ must be ≥ 0.25 to be resolved. However, the value of γ has no effects on the results and I have verified that, during the elastic regime, one obtains the same results with smaller values of $\Delta x = 0.05$ and 0.01 as well as smaller values of γ (Figure A1). However, because the time step is then extremely small, calculations take extremely long and the gravity current regime cannot be observed.

Appendix B: Axisymmetric Intrusion

[92] In this appendix, I consider the spreading of an axisymmetric flow of magma below a thin elastic plate of thickness d. Magma is injected at the center through a circular conduit of diameter a.

B1. Equations

[93] In cylindrical coordinates, the conservation of momentum in a thin elongated flow (as in section 3.1) leads to the following expression for the pressure P and radial velocity u within the flow:

$$P(r,z,t) = P_a + \rho_r g d + \rho_m g (h - z) + D\Delta_r^2 h \tag{B1}$$

$$u(r,z,t) = \frac{1}{2\mu}\frac{\partial P}{\partial r}\left(z^2 - hz\right) \tag{B2}$$

where D is the flexural rigidity of the plate and $\Delta_r^2 h = \frac{1}{r\partial r}\left(r\frac{\partial}{\partial r}\left(\frac{1}{r\partial r}\left(r\frac{\partial h}{\partial r}\right)\right)\right)$.

[94] Conservation of mass yields an equation for h, given an injection velocity w that corresponds to Poiseuille flow within a circular conduit of diameter a:

$$\frac{\partial h}{\partial t} = -\frac{1}{r}\frac{\partial}{\partial r}\left(r\int_0^h u(r,z,t)dz\right) + w(r,t) \tag{B3}$$

$$w(r,t) = \begin{cases} \dfrac{\Delta P^*}{4\mu Z_c}\left(\dfrac{a^2}{4} - r^2\right) & \text{if } r \le a/2 \\ 0 & \text{if } r > a/2 \end{cases} \tag{B4}$$

where ΔP^* is the effective overpressure driving the flow within the feeder conduit and is given by $\Delta P^* = \Delta P_c - \rho_m g h_0$ as in the Cartesian case.

[95] Using (B2) and (B1) in (B3), I find the following equation for the evolution of the thickness of the axisymmetric intrusion with time and radial coordinate:

$$\frac{\partial h}{\partial t} = \frac{\rho_m g}{12\mu r}\frac{\partial}{\partial r}\left(rh^3\frac{\partial h}{\partial r}\right) + \frac{D}{12\mu r}\frac{\partial}{\partial r}\left(h^3 r\frac{\partial}{\partial r}\left(\Delta_r^2 h\right)\right) + w(r,t) \tag{B5}$$

$$\frac{dV}{dt} = \frac{\pi a^4}{128\mu Z_c}\left(\Delta P_c - \rho_m g h_0(t)\right) \tag{B6}$$

The terms on the right hand side of (B5) represent (as in section 3.1.4) flow due to the own intrusion weight, flow due to the elastic response of the crust and injection rate. In cylindrical coordinates, radius, thickness and time scales are given by

$$R = \left(\frac{Ed^3}{12(1-\nu^2)\rho_m g}\right)^{1/4} \tag{B7}$$

$$H_r = a\left(\frac{3\Delta P_c}{32\rho_m g Z_c}\right)^{1/4} \tag{B8}$$

$$\tau_r = \frac{64\mu}{a^3}\left(\frac{3}{2}\right)^{1/4}\left(\frac{Ed^3}{12(1-\nu^2)}\right)^{1/2}\left(\frac{Z_c}{\Delta P_c \rho_m g}\right)^{3/4} \tag{B9}$$

respectively, where I use for the rate of injection: $Q_{0r} = \frac{\pi R^2 H_r}{\tau_r} = \frac{a^4 \pi \Delta P_c}{128\mu Z_c}$.

[96] Nondimensionalization of (B5) and (B6) using R, H_r and τ_r give the following dimensionless equations for the thickness and volume evolution in cylindrical coordinates for $0 \le r \le \gamma/2$:

$$\frac{\partial h}{\partial t} = \frac{1}{r}\frac{\partial}{\partial r}\left(rh^3\frac{\partial h}{\partial r}\right) + \frac{1}{r}\frac{\partial}{\partial r}\left(h^3 r\frac{\partial}{\partial r}\left(\Delta_r^2 h\right)\right) + \frac{32}{\gamma^2}\left(\frac{1}{4} - \frac{r^2}{\gamma^2}\right)\left(1 - \frac{h_0}{\sigma}\right) \tag{B10}$$

$$\frac{dV}{dt} = \left(1 - \frac{h_0}{\sigma}\right) \tag{B11}$$

where $\gamma = a/R$ and $\sigma = \Delta P_c/\rho_m g H_r$. For $r > \gamma/2$, the last term on the right side of (B10) is replaced by zero (no injection outside the conduit).

B2. Scaling Laws

[97] As in the Cartesian coordinates, I assume that, during a first phase, intrusion flow and morphology are controlled by the elastic response of the crust; the injection rate is constant and through a point source. In the elastic regime, the following equations thus hold:

$$\frac{\partial h}{\partial t} = \frac{1}{r}\frac{\partial}{\partial r}\left(h^3 r\frac{\partial}{\partial r}\left(\Delta_r^2 h\right)\right) \tag{B12}$$

$$\int_0^{r_N(t)} 2\pi r h(r,t)\,dr = t \tag{B13}$$

where $r_N(t)$ is the radius of the intrusion. I proceed as in section 5.1.1. to obtain the scaling law for h; that is, I look for a similarity solution for h in the form $f(\eta)t^\beta$, with $\eta = r/t^\alpha$ and, using (B13), I find that $\beta = 1 - 2\alpha$. Using this result in (B12), one obtains

$$t^{-2\alpha}\left((1-2\alpha)f - \alpha\eta\frac{df}{d\eta}\right) = t^{4-14\alpha}\frac{1}{\eta}\frac{d}{d\eta}\left(f^3\eta\frac{d}{d\eta}\Delta_\eta^2 f\right) \tag{B14}$$

which gives $\alpha = 1/3$ and $\beta = 1/3$ for a similarity solution to exist. The shape function $f(\eta)$ is then given by the solution of (B14) for $\alpha = 1/3$.

[98] This solution predicts that, during the first spreading phase, the elastic response of the crust is such that, for an axisymmetric flow, intrusion dimensions follow:

$$h_0 \propto t^{1/3} \tag{B15}$$

$$r_N \propto t^{1/3} \tag{B16}$$

$$h_0 \propto r_N \tag{B17}$$

with h_0 the maximum dimensionless thickness (thickness at the center) and r_N the dimensionless radius of the intrusion.

[99] When the volume becomes larger, previous results in cartesian coordinates show that the gravity current term dominates. In the gravity current regime, *Huppert* [1982] shows that for a constant injection rate, the radius of an axisymmetric flow follows:

$$r_N \propto t^{1/2} \tag{B18}$$

and that the maximum thickness stays constant with time and/or radius.

[100] In the regime of lateral propagation, I proceed as in section 5.3 to obtain a scaling law for the flow radius as a function of time. As in section 3.4, scaling analysis of (B10) and (B11) close to the current center gives

$$\frac{dh_s}{dt} = -\frac{h_s^4}{R_s^2} - \frac{h_s^4}{R_s^6} + \frac{8}{\gamma^2}\left(1 - \frac{h_s}{\sigma}\right) \tag{B19}$$

$$\frac{dV_s}{dt} = 1 - \frac{h_s}{\sigma} \tag{B20}$$

where subscript s stands for scale. Flow volume V_s can be approximated by the volume of a cylinder $\pi R_s^2 h_s$. In the regime of lateral propagation, $dh_s/dt \sim 0$ as $h_s \rightarrow \sigma$, the elastic term is negligible and the scaling law is obtained by equating the gravity current and the source terms, for which flexure of the elastic plate requires $\gamma \sim 1$:

$$\frac{h_s^4}{R_s^2} = 8\left(1 - \frac{h_s}{\sigma}\right) = 16\pi h_s R_s \frac{dR_s}{dt} \tag{B21}$$

$$\Rightarrow R_s^3 \frac{dR_s}{dt} = \frac{\sigma^3}{16\pi} \tag{B22}$$

$$\Rightarrow R_s \propto \left(\frac{\sigma^3 t}{4\pi}\right)^{1/4} \tag{B23}$$

Appendix C: Criterion for Fracture and Propagation of Lateral Intrusions

[101] The internal pressure required in a fluid-filled crack for the propagation of a magma fracture is given by [*Lister and Kerr*, 1991]

$$\Delta P_f \sim \frac{K_c}{l_d^{1/2}} \tag{C1}$$

where K_c is a critical stress intensity factor or fracture toughness of the order of 4 MPa.m$^{1/2}$ and l_d is the length of the crack.

[102] For large wavelength features, i.e., large values of l_d, such as in the laccolith case, the internal pressure required for magma propagation becomes small and the condition for failure is more easily met. However, as the flow length increases, the driving pressure of the flow decreases. In the elastic regime indeed, the homogeneous magma overpressure $\bar{P}$ that leads to the deformation of the elastic plate is given by (45) or (46); it decreases as l_d increases. Comparison of (46) with (C1) shows that the fracture propagates as long as

$$\bar{P} \geq \frac{K_c}{l_d^{1/2}} \tag{C2}$$

$$\Rightarrow l_d \leq \left(\frac{24 \times 0.4}{K_c}\right)^{4/9} \Lambda^{4/3} (\rho_m g)^{1/3} (12\mu Q_0)^{1/9} \tag{C3}$$

[103] One can calculate that the condition for fracture propagation is met as long as l_d is smaller than several tens of km, which is the case for lunar intrusive domes and terrestrial laccoliths. This result is in agreement with *Lister and Kerr* [1991], who have shown that the pressure required for fracture and continued propagation of sills is negligible compared to the elastic pressure.

[104] **Acknowledgments.** This paper has benefited from a careful review by Yanick Ricard and thoughtful comments by Mark Jellinek, Ross Kerr, and two anonymous reviewers. The author is also grateful for helpful discussions with Dave Bercovici and for his rereading of the manuscript. This work was supported by PNP/INSU/CNES and by Campus Spatial Paris Diderot. This is IPGP contribution 3127.

References

Annen, C. (2009), From plutons to magma chambers: Thermal constraints on the accumulation of eruptible silicic magma in the upper crust, *Earth Planet. Sci. Lett.*, *284*, 409–416.

Annen, C., and R. S. J. Sparks (2002), Effects of repetitive emplacement of basaltic intrusions on thermal evolution and melt generation in the crust, *Earth Planet. Sci. Lett.*, *203*, 937–955.

Bachmann, O., and G. W. Bergantz (2003), Rejuvenation of the Fish Canyon magma body: A window into the evolution of large-volume silicic magma systems, *Geology*, *31*, 789–792.

Barmin, A., O. E. Melnik, and R. S. J. Sparks (2002), Periodic behavior in lava dome eruptions, *Earth Planet. Sci. Lett.*, *199*, 173–184.

Bercovici, D. (1994), A theoretical model of cooling viscous gravity currents with temperature-dependent viscosity, *Geophys. Res. Lett.*, *21*, 1177–1180.

Bercovici, D., and J. Lin (1996), A gravity current model of cooling mantle plume heads with temperature-dependent buoyancy and viscosity, *J. Geophys. Res.*, *101*, 3291–3309.

Bruce, P. M., and H. E. Huppert (1989), Thermal controls of basaltic fissure eruptions, *Nature*, *342*, 665–667.

Canuto, C., M. Y. Hussaini, A. Quarteroni, and T. A. Zang (2007), *Spectral Methods: Evolution to Complex Geometries and Applications to Fluid Dynamics*, Springer, Berlin.

Coleman, D. S., W. Gray, and A. F. Glazner (2004), Rethinking the emplacement and evolution of zoned plutons: Geochronologic evidence for incremental assembly of the Tuolumne suite, California, *Geology*, *32*, 433–436.

Corazzato, C., and G. Gropelli (2004), Depth, geometry and emplacement of sills to laccoliths and their host-rock relationships: Montecampione group, southern Alps, Italy, in *Physical Geology of High-Level Magmatic Systems*, edited by C. Breitkreuz and N. Petford, *Geol. Soc. Spec. Publ.*, 234, 175–194.

Corry, C. E. (1988), *Laccoliths, Mechanics of Emplacement and Growths*, *Spec. Pap. Geol. Soc. Am.*, 220.

Crisp, J. A. (1984), Rates of magma emplacement and volcanic output, *J. Volcanol. Geotherm. Res.*, *20*, 177–211.

Cruden, A., and K. McCaffrey (2002), Different scaling laws for sills, laccoliths and plutons: Mechanical thresholds on roof lifting and floor depression, in *Physical Geology of Subvolcanic Systems - Laccoliths, Sills and Dykes (LASI)*, edited by A. M. C. Breitkreuz and N. Petford, *Geol. Soc. Spec. Publ.*, *234*, 15–17.

Del Gaudio, P., S. Mollo, G. Ventura, G. Iezzi, J. Tadeucci, and A. Cavallo (2010), Cooling rate-induced differentiation in anhydrous and hydrous basalts at 500 MPa: Implications for the storage and transport of magmas in dikes, *Chem. Geol.*, *270*, 164–178.

Elkins-Tanton, L., N. C. Chatterjee, and T. L. Grove (2003), Magmatic processes that produced lunar fire fountains, *Geophys. Res. Lett.*, *30*(10), 1513, doi:10.1029/2003GL017082.

Fialko, Y. (2001), On origin of near-axis volcanism and faulting at fast spreading mid-ocean ridges, *Earth Planet. Sci. Lett.*, *190*, 31–39.

Glazner, A., J. Bartley, D. Coleman, W. Gray, and R. Taylor (2004), Are plutons assembled over millions of years by amalgamation from small magma chambers?, *GSA Today*, *14*, 4–11.

Griffiths, R. W. (2000), The dynamics of lava flows, *Annu. Rev. Fluid Mech.*, *32*, 477–518.

Habert, G., and M. de Saint-Blanquat (2004), Rate of construction of the Black Mesa bysmalith, Henry Mountains, Utah, in *Physical Geology of High-Level Magmatic Systems*, edited by C. Breitkreuz and N. Petford, *Geol. Soc. Spec. Publ.*, 234, 163–173.

Head, J. W., et al. (2009), Evidence for intrusive activity on Mercury from the first MESSENGER flyby, *Earth Planet. Sci. Lett.*, *285*, 251–262, doi:10.1016/j.epsl.2009.03.008.

Horsman, E., B. Tikoff, and S. Morgan (2005), Emplacement-related fabric and multiple sheets in the Maiden Creek sill, Henry Mountains, Utah, USA, *J. Struct. Geol.*, *27*, 1426–1444.

Huppert, H. (1982), The propagation of two-dimensional and axisymmetric viscous gravity currents over a rigid horizontal surface, *J. Fluid Mech.*, *121*, 43–58.

Jackson, M. D., and D. D. Pollard (1988), The laccolith-stock controversy: New results from the southern Henry Mountains, Utah, *Bull. Geol. Soc. Am.*, *100*, 117–135.

Jellinek, A. M., and D. J. de Paolo (2003), A model for the origin of large silicic magma chambers: Precursors of caldera-forming eruptions, *Bull. Volcanol.*, *65*, 363–381.
Johnson, A., and D. Pollard (1973), Mechanics of growth of some laccolithic intrusions in the Henry Mountains, Utah, I. Field observations, Gilbert's model, physical properties and flow of the magma, *Tectonophysics*, *18*, 261–309.
Kavanagh, J. L., T. Menand, and R. S. J. Sparks (2006), An experimental investigation of sill formation and propagation in layered ealstic media, *Earth Planet. Sci. Lett.*, *245*, 799–813.
Kerr, A. D., and D. P. Pollard (1998), Toward more realistic formulations for the analysis of laccoliths, *J. Struct. Geol.*, *20*, 1783–1793.
Kerr, R. C., and J. R. Lister (1995), Comment on "On the relationship between dike width and viscosity", *J. Geophys. Res.*, *100*, 15,541.
Koch, F. G., A. M. Johnson, and D. D. Pollard (1981), Monoclinal bending of strata over laccolithic intrusions, *Tectonophysics*, *74*, 21–31.
Lister, J. R., and R. C. Kerr (1991), Fluid-mechanical models of crack propagation and their application to magma transport in dykes, *J. Geophys. Res.*, *96*, 10,049–10,077.
Mazzarini, F., G. Corti, G. Musumeci, and F. Innocenti (2004), Tectonic control on laccolith emplacement in the northern Apennines fold-thrust belt: the Gavorrano intrusion, southern Tuscany, Italy, in *Physical Geology of High-Level Magmatic Systems*, edited by C. Breitkreuz and N. Petford, *Geol. Soc. Spec. Publ.*, 234, 151–161.
McCaffrey, K. J. W., and N. Petford (1997), Are granitic intrusions scale invariant?, *J. Geol. Soc. London*, *154*, 1–4.
Menand, T. (2008), The mechanics and dynamics of sills in layered elastic rocks and their implications for the growth of laccoliths and other igneous complexes, *Earth Planet. Sci. Lett.*, *267*, 93–99, doi:10.1016/j.epsl.2007.11.043.
Metz, J. M., and G. A. Mahood (1991), Development of the Long Valley, California, magma chamber recorded in precaldera rhyolite lavas of Glass Mountain, *Contrib. Mineral. Petrol.*, *106*, 379–397.
Michaut, C., and D. Bercovici (2009), A model for the spreading and compaction of two-phase viscous gravity currents, *J. Fluid Mech.*, *630*, 299–399.
Michaut, C., and C. Jaupart (2006), Ultra-rapid formation of large volumes of evolved magma, *Earth Planet. Sci. Lett.*, *250*, 38–52.
Michaut, C., and C. Jaupart (2011), Two models for the formation of magma chamber by small increments, *Tectonophysics*, *500*, 34–49, doi:10.1016/j.tecto.2009.08.019.
Patankar, S. V. (1980), *Numerical Heat Transfer and Fluid Flow*, Taylor and Francis, Bristol, Pa.
Petford, N., and K. Gallagher (2001), Partial melting of mafic (amphibolitic) lower crust by periodic influx of basaltic magma, *Earth Planet. Sci. Lett.*, *193*, 483–499.
Petford, N., R. C. Kerr, and J. R. Lister (1993), Dike transport of granitoid magmas, *Geology*, *21*, 845–848.
Petford, N., R. C. Kerr, and J. R. Lister (1994), The ascent of felsic magmas in dykes, *Lithos*, *32*, 161–168.
Pollard, D., and A. Johnson (1973), Mechanics of growth of some laccolithic intrusions in the Henry Mountains, Utah, II. Bending and failure of overburden layers and sill formation., *Tectonophysics*, *18*, 311–354.
Rocchi, S., D. S. Westerman, A. Dini, F. Innocenti, and S. Tonarini (2002), Two-stage growth of laccoliths at Elba Island, Italy, *Geology*, *30*, 983–986.
Rubin, A. M. (1995), Propagation of magma-filled cracks, *Annu. Rev. Earth Planet. Sci.*, *23*, 287–336.
Schultz, P. H. (1976), Floor-fractured lunar craters, *Moon*, *15*, 241–273.
Shearer, C. K., et al. (2006), Thermal and magmatic evolution of the Moon, *Rev. Mineral. Geochem.*, *60*, 365–518, doi:10.2138/rmg.2006.60.4.
Sisson, T. W., T. L. Grove, and D. S. Coleman (1996), Hornblende gabbro sill complex at Onion Valley, California, and a mixing origin for the Sierra Nevada batholith, *Contrib. Mineral. Petrol.*, *126*, 81–108.
Stasiuk, M. V., C. Jaupart, and R. S. J. Sparks (1993), Influence of cooling on lava flow dynamics, *Geology*, *21*, 335–338.
Tait, S. R., C. Jaupart, and S. Vergniolle (1989), Pressure, gas content and eruption periodicity of a shallow, crystallising magma chamber, *Earth Planet. Sci. Lett.*, *92*, 107–123.
Turcotte, D. L., and G. Schubert (1982), *Geodynamics: Applications of Continuum Physics to Geological Problems*, John Wiley, New York.
Villeneuve, N., D. R. Neuville, P. Boivin, P. Bachèlery, and P. Richet (2008), Magma crystallization and viscosity: A study of molten basalts from the Piton de la Fournaise volcano (La Réunion island), *Chem. Geol.*, *256*, 242–251.
Wada, Y. (1994), On the relationship between dike width and magma viscosity, *J. Geophys. Res.*, *99*, 17,743–17,755.
Westerman, D. S., A. Dini, F. Innocenti, and S. Rocchi (2004), Rise and fall of a nested christmas-tree laccolith complex, Elba Island, Italy, in *Physical Geology of High-Level Magmatic Systems*, edited by C. Breitkreuz and N. Petford, *Geol. Soc. Spec. Publ.*, 234, 195–213.
Wieczorek, M. A., M. T. Zuber, and R. J. Phillips (2001), The role of magma buoyancy on the eruption of lunar basalts, *Earth Planet. Sci. Lett.*, *185*, 71–83.
Wilson, L., and J. W. Head (2003), Lunar Gruithuisen and Mairan domes: Rheology and mode of emplacement, *J. Geophys. Res.*, *108*(E2), 5012, doi:10.1029/2002JE001909.
Wilson, L., and J. W. Head (2008), Eruption rate of Mare lava flows on the Moon and implications for mantle melt volumes and dike geometries, *Lunar Planet. Sci.*, *XXXIX*, Abstract 1104.
Wöhler, C., R. Lena, P. Lazzarotti, J. Phillips, M. Wirths, and Z. Pujic (2006), A combined spectrophotometric and morphometric study of the lunar mare dome fields near Cauchy, Aragao, Hortensius and Milichius, *Icarus*, *183*, 237–264.
Wöhler, C., R. Lena, and J. Phillips (2007), Formation of lunar mare domes along crustal fractures: Rheologic conditions, dimensions of feeder dikes, and the role of magma evolution, *Icarus*, *189*, 279–307.
Wöhler, C., R. Lena, and Geologic Lunar Research Group (2009), Lunar intrusive domes: Morphometric analysis and laccolith modelling, *Icarus*, *204*, 381–398.
Wöhler, C., R. Lena, and K. C. Pau (2010), Lunar intrusive domes on the floor of Grimaldi and near Aristillus, *Lunar Planet. Sci.*, *XLI*, Abstract 1478.

C. Michaut, Equipe de Géophysique Spatiale et Planétaire, Institut de Physique du globe de Paris, UMR 7154, CNRS, Université Paris Diderot, Sorbonne Paris Cité, F-94107 Saint-Maur-des-Fossés, France. (michaut@ipgp.fr)